Cell

Z-form extracellular DNA is a structural component of the bacterial biofilm matrix

Graphical abstract

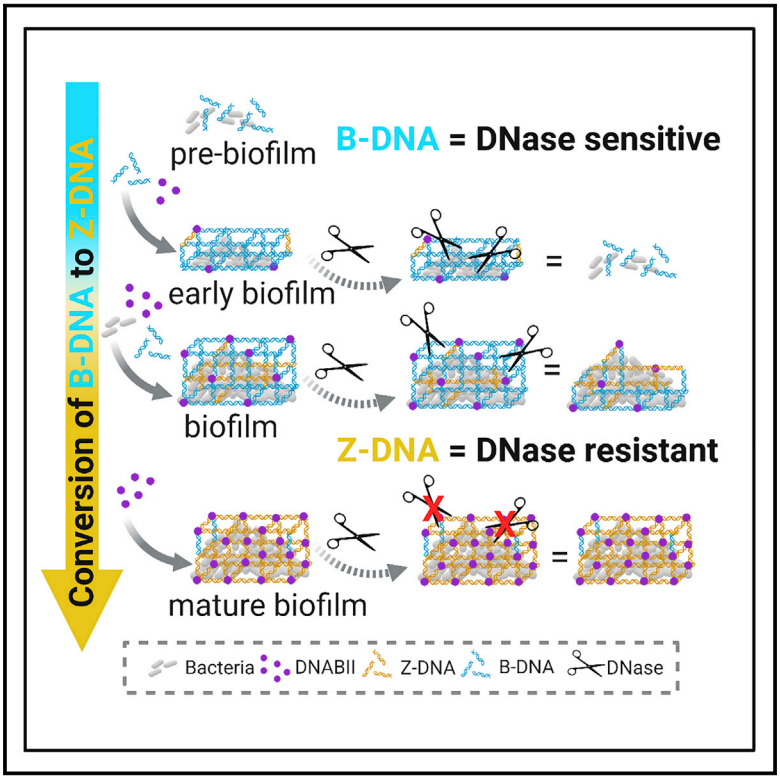

Authors

John R. Buzzo, Aishwarya Devaraj, Erin S. Gloag, ..., Paul Stoodley, Lauren O. Bakaletz, Steven D. Goodman

Correspondence

lauren.bakaletz@nationwidechildrens.org (L.O.B.), steven.goodman@nationwidechildrens.org (S.D.G.)

In brief

The structural integrity of bacterial biofilms is strengthened by the action of bacterial DNABII proteins that drive the accumulation of extracellular, nuclease-resistant Z-form DNA and inhibit host neutrophil extracellular trap function.

Highlights

- Z-DNA is stable and abundant extracellularly
- Z-DNA provides structure and DNase-resistance to the biofilm matrix
- Bacterial DNABII proteins mitigate NET function

Buzzo et al., 2021, Cell *184*, 5740–5758
November 11, 2021
https://doi.org/10.1016/j.cell.2021.10.010

CellPress

CellPress
OPEN ACCESS

Cell

Article

Z-form extracellular DNA is a structural component of the bacterial biofilm matrix

John R. Buzzo,[1] Aishwarya Devaraj,[1] Erin S. Gloag,[2] Joseph A. Jurcisek,[1] Frank Robledo-Avila,[1] Theresa Kesler,[1] Kathryn Wilbanks,[1] Lauren Mashburn-Warren,[3] Sabarathnam Balu,[1] Joseph Wickham,[1] Laura A. Novotny,[1] Paul Stoodley,[2,4,5] Lauren O. Bakaletz,[1,6,*] and Steven D. Goodman[1,6,7,*]

[1]Center for Microbial Pathogenesis, Abigail Wexner Research Institute at Nationwide Children's Hospital, Columbus, OH 43205, USA
[2]Department of Orthopedics, Ohio State University, Columbus, OH 43210, USA
[3]The Steve and Cindy Rasmussen Institute for Genomic Medicine, Abigail Wexner Research Institute at Nationwide Children's Hospital, Columbus, OH 43205, USA
[4]Department of Microbial Infection and Immunity, Ohio State University, Columbus, OH 43210, USA
[5]National Centre for Advanced Tribology at Southampton, University of Southampton, Southampton S017 1BJ, UK
[6]Department of Pediatrics, College of Medicine, Ohio State University, Columbus, OH 43210, USA
[7]Lead contact
*Correspondence: lauren.bakaletz@nationwidechildrens.org (L.O.B.), steven.goodman@nationwidechildrens.org (S.D.G.)
https://doi.org/10.1016/j.cell.2021.10.010

SUMMARY

Biofilms are community architectures adopted by bacteria inclusive of a self-formed extracellular matrix that protects resident bacteria from diverse environmental stresses and, in many species, incorporates extracellular DNA (eDNA) and DNABII proteins for structural integrity throughout biofilm development. Here, we present evidence that this eDNA-based architecture relies on the rare Z-form. Z-form DNA accumulates as biofilms mature and, through stabilization by the DNABII proteins, confers structural integrity to the biofilm matrix. Indeed, substances known to drive B-DNA into Z-DNA promoted biofilm formation whereas those that drive Z-DNA into B-DNA disrupted extant biofilms. Importantly, we demonstrated that the universal bacterial DNABII family of proteins stabilizes both bacterial- and host-eDNA in the Z-form *in situ*. A model is proposed that incorporates the role of Z-DNA in biofilm pathogenesis, innate immune response, and immune evasion.

INTRODUCTION

Bacterial biofilms are comprised of a community of cells either aggregated or attached to a surface, which are embedded in a self-produced extracellular polymeric substance (EPS) matrix. This EPS contains extracellular DNA (eDNA), proteins, lipids, polysaccharides, biopolymers, and divalent cations and provides a protective barrier against harsh environments, antimicrobials, and host immune effectors (Flemming and Wingender, 2010; Koo et al., 2017). Universally, the structure of eDNA is maintained by the two-member DNABII family of proteins (Devaraj et al., 2018), integration host factor (IHF) and histone-like protein (HU), of which at least one allele is present in the genomes of all eubacteria (Dey et al., 2017). The DNABII proteins bind to and bend DNA with high affinity (Swinger and Rice, 2004) and serve as accessory proteins in multiple nucleoprotein interactions within the bacterial cell (Grove, 2011; Mangan et al., 2006). We have previously shown that these proteins also serve a role extracellularly, wherein they act as linchpin proteins to stabilize the crossed-strand structure of eDNA, and these eDNA structures functionally resemble Holliday junctions (HJs) (Devaraj et al., 2019) within the biofilm EPS and are required for the stability of the biofilm matrix (Brockson et al., 2014; Devaraj et al., 2018). Targeted removal of DNABII proteins with specific antibodies results in rapid, significant biofilm collapse (Devaraj et al., 2015; Gunn et al., 2016; Novotny et al., 2013a; Rocco et al., 2018) with release of resident bacteria that are markedly more susceptible to antibiotics and host immune effectors (Brockson et al., 2014; Gunn et al., 2016; Mokrzan et al., 2020a; Novotny et al., 2013a).

eDNA is a ubiquitous component of the biofilm EPS and is compositionally similar to fragmented intracellular genomic DNA (Steinberger and Holden, 2005). Several studies have shown that nuclease-mediated degradation of eDNA will indeed prevent biofilm formation (Frederiksen et al., 2006; Gunn et al., 2016; Martins et al., 2012; Whitchurch et al., 2002). However, these nucleases typically have no obvious effect on mature *in vitro* (e.g., >24 h) biofilms, even though eDNA remains a dominant matrix component (Gunn et al., 2016; Hall-Stoodley et al., 2008; Kaplan et al., 2012; Koo et al., 2017; Novotny et al., 2013a; Saunders et al., 2020). The reason for this nuclease-resistant state of mature biofilms remains uncharacterized and is the focus of our work described here.

DNA in the B-form adopts a right-handed, low energy configuration that is sensitive to nuclease degradation and is the most common DNA configuration under physiologic conditions (Bezanilla et al., 1994; Suck and Oefner, 1986). Conversely, Z-DNA has a left-handed configuration with distinct nucleotide geometry but

preserves Watson-Crick base-pairing, is resistant to nuclease degradation (Ramesh and Brahmachari, 1989), and is not abundant intracellularly due to its high intrinsic energy state (Dumat et al., 2016; Ho et al., 1991; Kim et al., 2018). However, Z-DNA-forming sequences are involved in multiple intracellular transactions (Zavarykina et al., 2019; Shin et al., 2016; Zhou et al., 2009; Ray et al., 2013; Wang et al., 2006; van der Vorst et al., 2018). Additionally, Z-DNA binding proteins, although rare, are involved in gene regulation (Oh et al., 2002), viral pathogenesis (e.g., E3L) (Kim et al., 2003; Kwon and Rich, 2005), innate immune sensing (e.g., ZBP1) (Kuriakose and Kanneganti, 2018; Newton et al., 2016), DNA recognition (e.g., ADAR-1) (Kim et al., 2000), and inflammation (Szczesny et al., 2018). There is also ample experimental evidence of Z-DNA formation in the presence of high ionic strength (Ali and Ali, 1997; Peck et al., 1982), Z-DNA binding proteins (Bae et al., 2011), negative supercoiling (Nordheim et al., 1982; Nordheim and Rich, 1983; Wittig et al., 1991), as well as induction of Z-DNA via nucleotide modification (e.g., methylation and or bromination) that can reduce the high energy activation barrier (Temiz et al., 2012). Although there are Z-prone DNA sequences (e.g., alternating dGdC) (Möller et al., 1982), all sequences of DNA are capable of conversion to the Z-form (Kypr et al., 2009). Despite recent advances in Z-DNA research, no extracellular role had yet been discovered.

Although no studies have provided evidence of non B-form DNA structures involved with biofilm stability (Kassinger and van Hoek, 2020), a recent publication does show the presence of B-form G-quadraplex structures that contribute to the structure of *Pseudomonas aeruginosa* biofilms (Seviour et al., 2021), thus highlighting the complex architectural eDNA structures of bacterial biofilms. Z-DNA is the most common conformation of DNA that is nuclease-resistant (Ramesh and Brahmachari, 1989; Thomas et al., 1985; Zhang et al., 2019). We thereby hypothesized that in mature bacterial biofilms, eDNA was in the Z-form. To examine this premise, we showed abundant Z-DNA within biofilms formed by multiple human pathogens *in vitro*, as well as within biofilm fragments present in clinical specimens. We used DNase treatment to distinguish the contribution of B-DNA versus Z-DNA to biofilm stability, and further, used compounds known to induce or revert Z-DNA to the B-form (and vice versa), to determine whether conversion of eDNA to B- or Z-forms affected biofilm architecture and/or mechanical properties. Our study provided compelling evidence of a stable presence of Z-DNA as a structural component of mature biofilms. Furthermore, Z-DNA confers the observed nuclease-resistance to these structures and thus contributes significantly to the recalcitrance of eDNA-dependent bacterial biofilms. Importantly, we demonstrated that bacterial DNABII proteins inactivated NET-mediated bacterial killing function of polymorphonuclear leukocytes (PMNs) through conversion of host-derived B-DNA to Z-DNA.

RESULTS

Z-DNA was present in all tested biofilms

DNase added at biofilm initiation, but not when mature, significantly inhibits biofilm formation (Frederiksen et al., 2006; Martins et al., 2012; Whitchurch et al., 2002; Gunn et al., 2016; Hall-Stoodley et al., 2008; Kaplan et al., 2012). We recapitulated this phenomenon here with three human pathogens: uropathogenic *E. coli* (UPEC), Klebsiella *pneumoniae* (*Kp*), and nontypeable *Haemophilus influenzae* (NTHI). Whereas Pulmozyme, a DNase commonly used to debulk mucus and resident bacteria within the lungs of people with cystic fibrosis (CF) (Frederiksen et al., 2006) prevented biofilm formation, mature biofilms were resistant (Figures S1A and S1B).

We previously showed that eDNA is both present in mature biofilms and an integral component of the EPS structure (Devaraj et al., 2015; Novotny et al., 2013a; Novotny et al., 2013b; Rocco et al., 2017). DNase readily degrades double-stranded DNA (dsDNA), and to a lesser degree single-stranded DNA (ssDNA) (Baranovskii et al., 2004), but not Z-DNA (Ramesh and Brahmachari, 1989). Although ssDNA is important for the initial phase of *Neisseria gonorrhea* biofilm formation, only dsDNA was important for its biofilm structure (Zweig et al., 2014). We thereby hypothesized that the inability of DNase to affect mature biofilms was likely due to a nuclease-resistant DNA conformation (e.g., Z-DNA). To determine the presence of Z-DNA, we performed immunofluorescence (IF) microscopy using monoclonal antibodies (mAbs). We first validated the specificity of these mAbs against a Z-DNA substrate (brominated poly(dGdC)) (Edgington and Stollar, 1992) (Figure S2A) by ELISA (Figures S2B and S2C) and confirmed no cross-reactivity to whole cell lysates of NTHI by western blot (Figure S2D). We then showed that NTHI genomic (gDNA) could be converted to Z-DNA in a non-sequence-specific manner by bromination in the presence of 3.6 M NaCl (Figure S2E). Last, we confirmed the resistance of brominated poly(dGdC) (Z-DNA) to degradation by DNase (Figure S2F).

Via use of these highly specific mAbs directed against B-DNA (Heegaard et al., 1996) or Z-DNA (Möller et al., 1982), we first assessed whether Z-DNA was present in biofilms formed by several well-known biofilm-forming pathogens: NTHI, UPEC, *Kp*, *P. aeruginosa*, and *Streptococcus mutans* using IF. Strikingly, abundant levels of both B-DNA and Z-DNA were present within the EPS of the mature biofilms (40 h) formed by all pathogens tested (Figure 1A). Furthermore, we showed that although both Z-DNA and B-DNA increased within the EPS of biofilms formed over time (24 h, 40 h, and 90 h) by NTHI, *Kp*, and UPEC, after 1 week, eDNA in biofilms formed by NTHI was so strongly skewed to the Z-DNA form that the B-DNA signal was below the level of detection (Figures S3A and S3B). Additionally, we confirmed that there is no secondary antibody cross-reactivity (e.g., nonspecific fluorescence) within NTHI biofilms (Figure S3C). This finding demonstrates that, at least *in vitro*, as biofilms mature, Z-DNA continues to accumulate.

Next, we examined the DNA content of biofilms formed on primary, polarized human airway epithelial cells (HAEs), as a bridge to *in vivo* experiments. We allowed the airway pathogen, NTHI (Mokrzan et al., 2016) to form a 16 h biofilm on polarized HAEs (Figure 1B) (Mokrzan et al., 2020b; Zhang et al., 2002) and then probed for both B-DNA and Z-DNA by IF. In the absence of NTHI, no visible eDNA strands were observed (Figure 1C). In contrast, in HAEs with an apically formed NTHI biofilm, eDNA strands of both B- and Z-DNA were observed (Figure 1D). This result further confirmed that in all cases tested, Z-form DNA was present during biofilm formation.

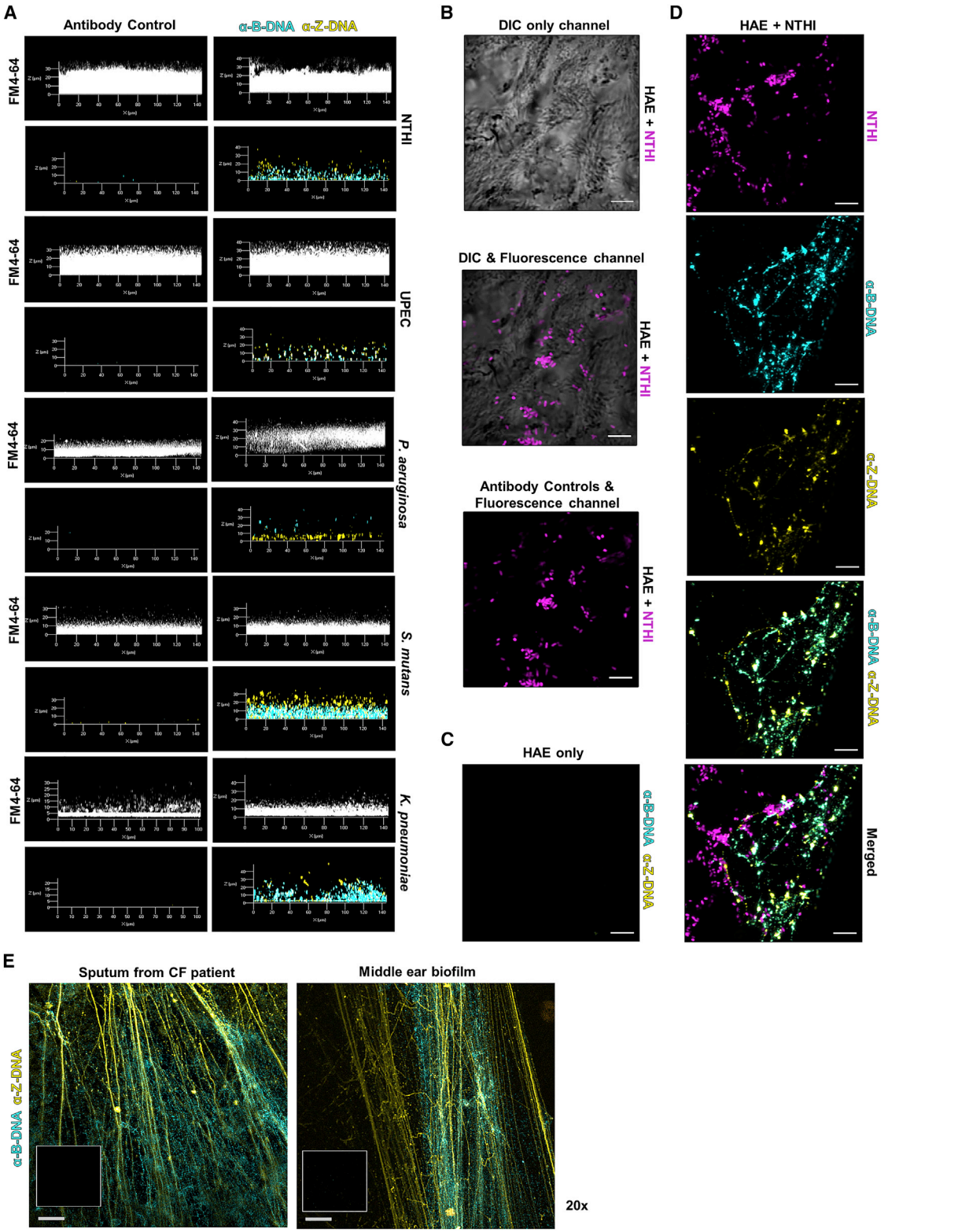

Figure 1. Z-DNA was present in biofilms formed by multiple bacterial species *in vitro* and *in vivo*

(A) Both B- and Z-DNA were present in biofilms. NTHI, UPEC, *P. aeruginosa*, *S. mutans*, and *K. pneumoniae* biofilms were established for 40 h. Unfixed biofilms were incubated with rabbit monoclonal antibody against Z-DNA(Z22) (5 μg/mL) a murine monoclonal antibody against B-DNA(3519) (5 μg/mL), murine isotype

(legend continued on next page)

We then determined by IF whether Z-DNA was also present in *ex vivo* biofilms recovered from the middle ear of a chinchilla with experimental otitis media due to NTHI and examined sputum expectorated from a person with CF that was culture-positive for both methicillin-susceptible *Staphylococcus aureus* (MSSA) and *Burkholderia cenocepacia.* As shown in Figure 1E, Z-DNA (yellow) was abundant within these single- and mixed-species biofilm fragments. Z-DNA was visualized as thick, fiber-like strands, which is a characteristic of Z-DNA (Chaires and Norcum, 1988) and was similar to that observed within biofilms formed on HAEs *in vitro* (Figure 1D). Collectively, these data demonstrated Z-DNA as a component of the EPS of biofilms formed as part of the bacterial disease course.

Z-DNA was the primary structural form of eDNA within mature biofilms

We expanded our hypothesis to consider that in addition to DNase-resistance, Z-DNA and not B-DNA, served as an important structural form of eDNA. To test this hypothesis, we allowed NTHI, *Kp*, and UPEC to form mature biofilms *in vitro* for 24 h, followed by incubation with DNase for 16 h. We then quantified the relative B-DNA and Z-DNA content by IF microscopy, wherein fluorescence intensity was normalized against fluorescently labeled biofilm cells. As shown in Figure 2A, although B-DNA levels were significantly reduced after incubation with DNase, Z-DNA levels were maintained. A comparison of the ratio of B-DNA and Z-DNA fluorescence in DNase-treated biofilms to their respective controls (untreated biofilms) demonstrated a notable shift toward a biofilm wherein Z-DNA was the predominant form (Figure 2B). Additionally, NTHI biofilms were incubated for 40 h in the presence of DNase throughout biofilm development, and the relative B-DNA and Z-DNA content was quantified as described above. These data showed a statistically significant decrease in average thickness, a marked reduction in Z-DNA, and near abolishment of B-DNA, with a Z/B-DNA ratio that strongly favored Z-DNA (Figures S4A–S4D). This finding suggests that the addition of DNase degrades B-DNA during biofilm development that lessens the production of Z-DNA. However, once formed, Z-DNA was not vulnerable to DNase. These data also support the concept that Z-DNA could provide a mode of DNase resistance that was not due to protease inactivation (Saunders et al., 2020; Whitchurch et al., 2002). Collectively, these data suggested that B-DNA served as a reservoir of eDNA for Z-DNA formation, and nuclease-resistant Z-DNA, not B-DNA, was critical to maintain the stability of bacterial biofilms.

Z-DNA-specific antibodies stimulated biofilm formation

Z-DNA-binding proteins (Bae et al., 2011; Kim et al., 2018), which include Z-DNA-specific antibodies, bind to and/or stabilize Z-form DNA structure (Lafer et al., 1985; Moinuddin et al., 1998) and thus also shift the B/Z DNA equilibrium toward the Z-DNA conformation (Lafer et al., 1986; Lee et al., 2018). We thereby hypothesized that the addition of Z-DNA-specific antibodies would stabilize and shift the equilibrium of eDNA to favor the Z-conformation and facilitate biofilm formation. To this end, we added purified IgG isolated from Z-DNA-specific polyclonal (Safina et al., 2017) antibodies (pAB), as well as a specific Z-DNA mAb (Thomas et al., 1991) to cultures of NTHI and/or UPEC at the time of biofilm initiation. As seen in Figures S5A and S5B, addition of either polyclonal or monoclonal Z-DNA-specific antibodies induced a significant, dose-dependent increase in biofilm average thickness.

A shift in B/Z equilibrium of eDNA modulated biofilm structure

The equilibrium of B-DNA to Z-DNA conversion is also facilitated in the presence of multi-valent cations or high ionic strength (Pohl and Jovin, 1972), whereas the binding of intercalating agents tend to favor the B-DNA conformation (Mirau and Kearns, 1983). We used these principles to attempt to drive eDNA into either the B- or Z-forms to determine if either state was preferentially associated with biofilm formation. To drive B-DNA into Z-DNA, we utilized the ability of cerium (III) chloride ($CeCl_3$) to form self-assembled Z-DNA aggregate structures at low concentrations (<1 mM). $CeCl_3$ binds to the phosphate backbone of DNA, which thus neutralizes the electrostatic repulsion, allowing the Z-DNA form to be energetically favored (Bhanjadeo et al., 2017). We first confirmed that $CeCl_3$ induced conversion of gDNA to Z-form (Bhanjadeo et al., 2017) in a dose-dependent manner by spectroscopic A260/295 absorbance ratio assay (Thomas and Messner, 1988) (Figure S5C). To now determine whether $CeCl_3$ altered the Z-DNA content of biofilms, mature NTHI biofilms were incubated with increasing concentrations of $CeCl_3$, then probed for the presence of Z-DNA by IF

IgG2a, and IgG purified from unimmunized rabbit serum (5 μg/mL). Then, biofilms were incubated with goat α-mouse IgG conjugated Alexa Fluor 405 (cyan) and goat α-rabbit IgG conjugated Alexa Fluor 488 (yellow), and counterstained with bacterial membrane stain FM4-64 (white). NTHI, n = 3; UPEC, n = 3; *Pa*, n = 4; *S. mu*, n = 3; *Kp*, n = 4.

(B) NTHI biofilms could be readily established on human airway epithelial cells (HAEs) NTHI (pMDC-P1, a GFP reporter isolate [fuchsia]) biofilms were established for 16 h on primary HAEs (gray), which were incubated with murine IgG1, IgG purified from unimmunized rabbit serum as negative controls. Differential interference contrast (DIC) microscopy was used to visualize HAEs.

(C) B- and Z-DNA could be visualized on HAEs but only when NTHI biofilms were present. No fluorescent signal was detected when HAEs only (no NTHI inoculated) were labeled with B4- and Z-DNA-specific monoclonal antibodies (as described in A) followed by goat-α-rabbit IgG conjugated Alexa Fluor (yellow), and goat-α-mouse IgG-conjugated Alexa Fluor 594 (cyan).

(D) NTHI biofilms formed on HAEs immunolabeled for B-DNA and Z-DNA, as described above. Individual and merged fluorescent channel images shown. (B–D) Representative images shown, scale bars, 5 μM (n = 6).

(E) Representative images of immunohistochemical labeling of B-DNA with murine α-B-DNA(3519) and Z-DNA with rabbit αZ-DNA(Z22) in specimens collected during experimental and clinical diseases. Labeling was revealed with goat anti-rabbit IgG conjugated to Alexa Fluor 647 and/or goat anti-mouse IgG conjugated to Alexa Fluor 488. Left: sputum from an individual with cystic fibrosis (n = 7). Right: NTHI biofilm formed for 14 days within the middle ear of a chinchilla with experimental otitis media (n = 2). Insets: negative control murine monoclonal antibody isotype IgG2a and IgG from unimmunized rabbit serum. Scale bar, 10 μm. See also Figures S2 and S3.

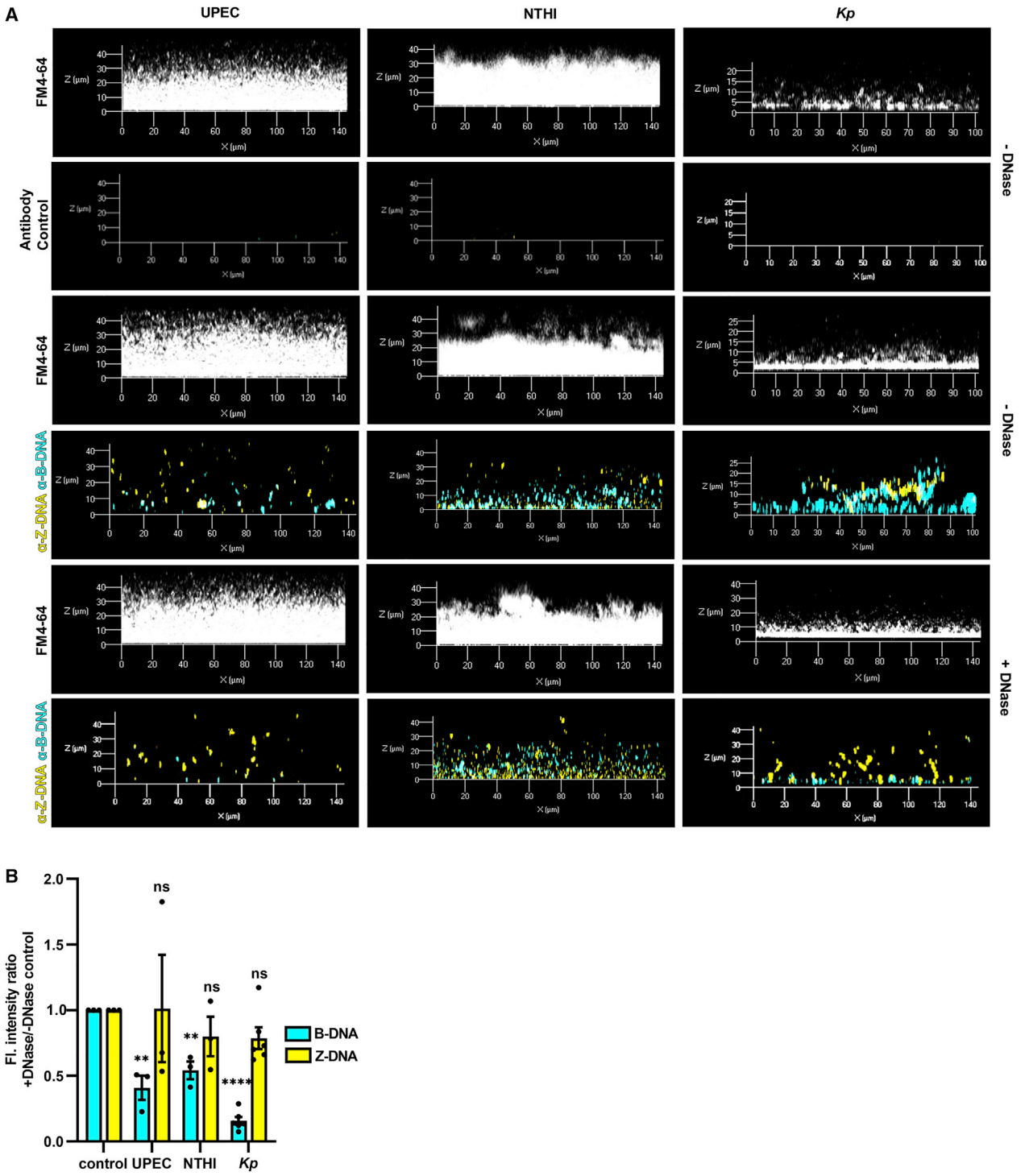

Figure 2. Z-DNA remained intact after DNase treatment

(A) UPEC, NTHI, and *K. pneumoniae* were allowed to form biofilms for 24 h then incubated with DNase (Pulmozyme; 40 U/mL in media) for 16 h. Biofilms were then incubated with murine monoclonal raised against B-DNA(3519) (5 μg/mL) and rabbit monoclonal antibody raised against Z-DNA(Z22) (5 μg/mL) or IgG2a and IgG purified from unimmunized rabbit serum, then counterstained with FM 4-64.

(B) Changes in abundance of B-DNA or Z-DNA after DNase treatment were quantified as the ratio of fluorescence intensity (FI) of B-DNA or Z-DNA compared to untreated biofilms (−DNase) using ImageJ software. FI was normalized to total biomass (FM4-64 fluorescent signal). Error bars represent the SEM. UPEC, n = 3; NTHI, n = 3; *Kp*, n = 6. Statistical significance compared to control (−DNase) was assessed by paired t tests, **p < 0.01; ****p < 0.0001.

See also Figures S1 and S4.

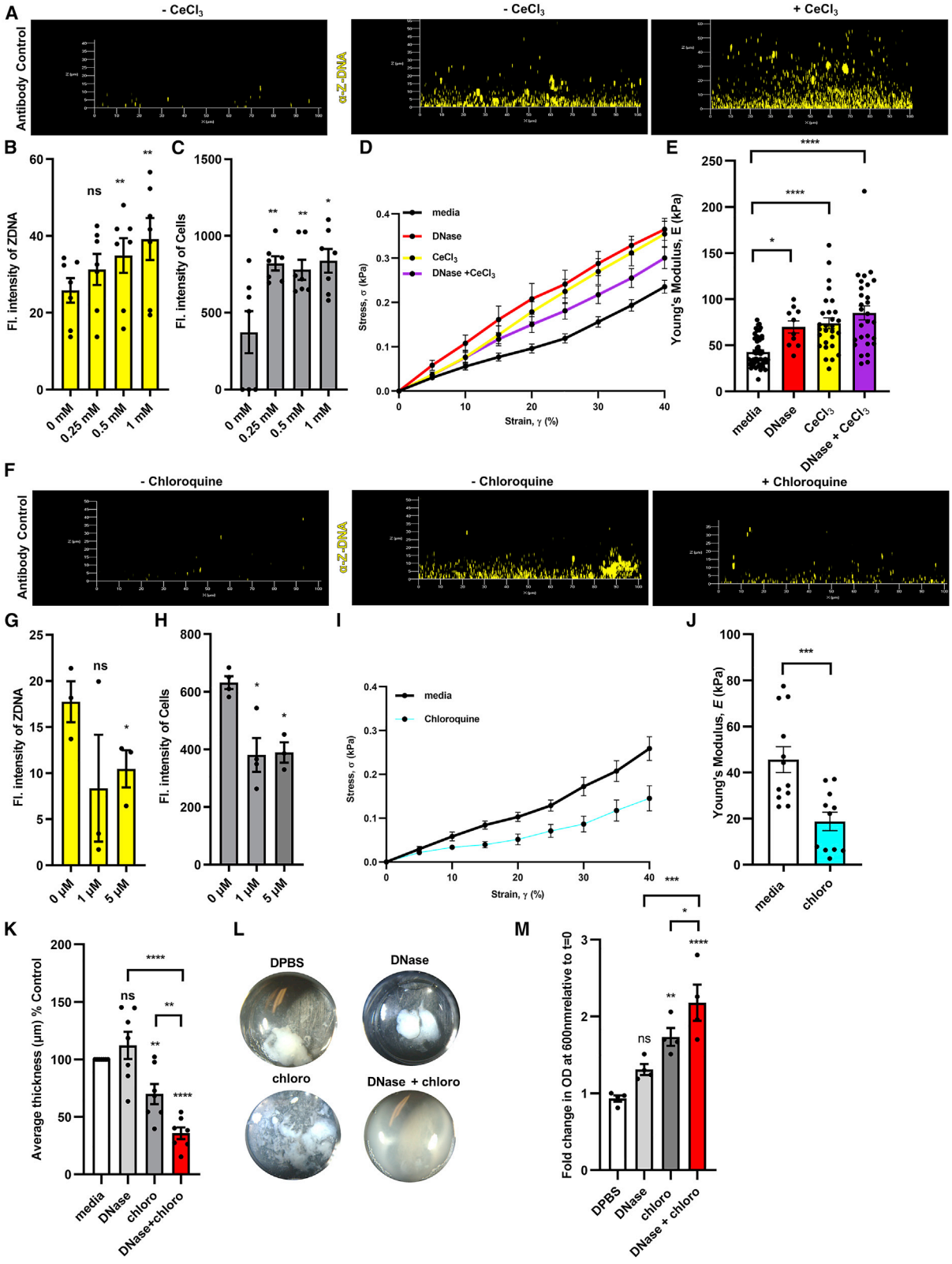

(legend on next page)

microscopy. As shown in Figures 3A and 3B, $CeCl_3$ induced an increase in Z-DNA signal and a dose-dependent increase in overall fluorescent intensity of bacterial biomass (Figure 3C). We confirmed that $CeCl_3$ did not negatively affect NTHI planktonic growth (Figure S5D) but resulted in a greater proportion of bacteria that favored the biofilm state (Figure S5E). These results suggested that an equilibrium shift from B-DNA to Z-DNA enhanced biofilm formation by promoting a biofilm dominant state over planktonic growth.

We then used rheological analysis to determine if DNase (removal of B-DNA) and/or $CeCl_3$ (induction of Z-DNA) altered the bulk mechanical properties of a biofilm, using NTHI as a model. We performed axial mechanical indentation on untreated (media) biofilms and those incubated with DNase, $CeCl_3$, or a sequential addition of both (e.g., induction of Z-DNA followed by removal of B-DNA) wherein an 8-mm geometry was lowered onto the biofilm, using an approach rate of 1 μm/s, and the force required to compress the biofilm was determined (Devaraj et al., 2019). From the stress-strain curves, there was a significant difference in the mechanical properties between all three treatments compared to untreated biofilms (Figure 3D). The Young's modulus, an indication of how stiff a material is in response to a normal force (Timoshenko and Goodier, 1970), was determined at the lower linear portion of the force-displacement curve (see Equation S1 in section "axial mechanical indentations of NTHI biofilms" in the STAR Methods) as demonstrated in Figure S5F. In support of our observations from the stress-strain curves, there was a significant statistical difference between the Young's modulus and all three conditions compared to control biofilms (Figure 3E). These data indicated that DNase, $CeCl_3$, and $CeCl_3$+DNase resulted in an increased Young's modulus that is indicative of a more rigid biofilm. This outcome suggested that reduction of the proportion of B-DNA (e.g., via incubation with Pulmozyme), without affecting the steady-state levels of Z-DNA, increased the stiffness and thus, the stability of the biofilm EPS. Additionally, incubation of DNase after conversion to Z-DNA (e.g., $CeCl_3$-treated) demonstrated no change in rigidity, which suggested that the mode of action of $CeCl_3$ treatment on biofilms was directed toward eDNA. Taken together, we concluded that the stiffness of the biofilm could be attributed to eDNA being solely in the Z-form.

To drive Z-DNA into B-DNA, we utilized the DNA-intercalating agent chloroquine, which prevents the formation of Z-DNA (Kwakye-Berko and Meshnick, 1990). We hypothesized that chloroquine, an immunosuppressant drug used for the prevention and treatment of malaria, as well as for disorders such as systemic lupus erythematosus (SLE) (Al-Bari, 2015), would shift the B-Z equilibrium of mature biofilms to primarily the B-form and thus reduce biofilm structural integrity. We first confirmed that chloroquine prevented NaCl-induced Z-DNA conversion by spectroscopic absorbance ratio assay (Figure S5G) and further showed there was no effect on NTHI growth (Figure S5H). We allowed NTHI to establish a biofilm (24 h) followed by incubation with increased concentrations of chloroquine (at concentrations that had no effect on NTHI growth) and then probed for the presence of Z-DNA by IF. Chloroquine caused a significant reduction in overall Z-DNA signal and a dose-dependent decrease of NTHI in the biofilm state, which suggested that Z-DNA was critical for biofilm stabilization (Figures 3F–3H). Moreover, we observed that chloroquine partitioned biofilm-resident bacteria toward the planktonic state (Figure S5I), which suggested that the DNA-intercalating effects of chloroquine drove Z-DNA into B-DNA, thus likely disrupting the biofilm EPS that lead to the release of bacteria from biofilm residence without

Figure 3. B/Z eDNA ratio modulates the physical properties of biofilms

NTHI biofilms formed for 24 h were incubated with $CeCl_3$ (500 μM) for 16 h, then incubated with unimmunized rabbit IgG (5 μg/mL) or rabbit α-Z-DNA(Z22) (5 μg/mL), and then with goat α-rabbit IgG conjugated with Alexa Fluor 488 and imaged by CLSM.

(A) Representative image of an NTHI biofilm with 500 μM $CeCl_3$.

(B and C) ImageJ quantifications of Z-DNA (Alexa Fluor 488) and bacterial cells (FM4-64) signal intensities. Statistical significance compared to control was assessed by paired t tests, *$p < 0.05$, **$p < 0.01$, $n = 7$. To determine the mechanical properties of biofilms, NTHI biofilms were formed for 24 h on glass fluorodishes and then incubated with media or 500 μM $CeCl_3$ for 16 h at 37°C. Additionally, 24 h biofilms were incubated with media or $CeCl_3$ for 16 h and then treated with Pulmozyme (50 μg/mL) for 1 h.

(D) Stress-strain curves of NTHI biofilms were determined from axial mechanical indentation analysis.

(E) Young's modulus was determined from the lower linear region of the stress-strain curve depicted in (D). Statistical significance determined by one-way ANOVA. *$p < 0.05$, ns; not significant compared to media only control. NTHI biofilms formed for 24 h were incubated with chloroquine (5 μM) for 16 h then incubated with unimmunized rabbit IgG (5 μg/mL) or rabbit α-Z-DNA(Z22) (5 μg/mL) and then with goat α-rabbit IgG conjugated with Alexa Fluor 488 and imaged by CLSM.

(F) Representative image of an NTHI biofilm with 5 μM chloroquine.

(G and H) ImageJ quantifications of Z-DNA (Alexa Fluor 488) and bacterial cells (FM4-64) in the presence of chloroquine. Statistical significance compared to control was assessed by paired t tests, *$p < 0.05$, **$p < 0.01$, $n = 3$. Mechanical properties of 40 h NTHI biofilms formed on glass fluorodishes and incubated with media or chloroquine (5 μM) for 1 h at 37°C.

(I) Stress-strain curves of NTHI biofilms treated with chloroquine were determined as described previously (D).

(J) Young's modulus was determined as described in (E) from stress-strain curve in (G). Statistical significance determined by one-way ANOVA or unpaired t test *$p < 0.05$; ns, not significant compared to media only control; $n = 3$ (2 biofilms for each replicate was analyzed for a total of 6 biofilms per group).

(K–M) Modulation of B/Z eDNA increased the susceptibility of biofilms to DNase after treatment with chloroquine.

(K) NTHI biofilms were formed for 40 h and incubated with chloroquine, DNase, or both, then stained with LIVE/DEAD, fixed, visualized via CLSM, and images analyzed by COMSTAT. Average thickness as a percent of media control, $n = 7$.

(L) Images of the sputum solids disruption assay ($n = 1$) where clinical sputum exudates were incubated with DPBS (control), chloroquine (100 μM), DNase (30 U), or in combination for 1 h at 37°C, then analyzed for change in OD_{600} over time, $n = 4$.

(M) Fold change in OD_{600} relative to t = 0. Higher OD_{600} relative to t = 0 indicates biofilm disruption. Scale bar, 10 μm. Error bars represent the SEM. Statistical significance compared to control was assessed by unpaired t tests, *$p < 0.05$, **$p < 0.01$, ***$p < 0.001$, ****$p < 0.0001$, $n = 4$.

See also Figures S5 and S6 and Table S1.

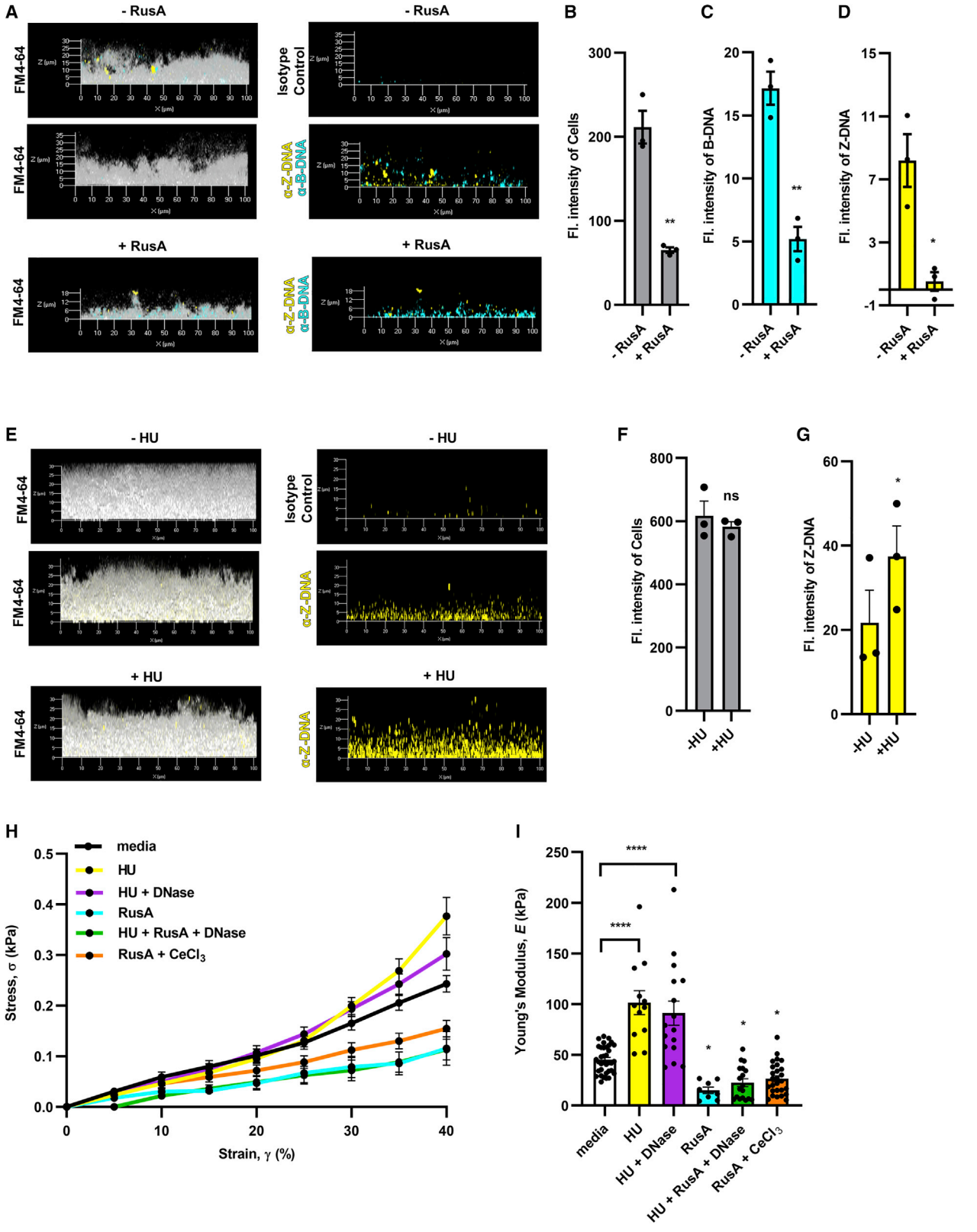

(legend on next page)

cell killing. We also performed rheological analysis to determine how the conversion of Z-DNA to B-DNA affected biofilm mechanics. Axial mechanical indentation was performed on untreated NTHI biofilms (media) or those incubated with chloroquine, as described above. Stress-strain analysis indicated that the mechanics of chloroquine-incubated biofilms were altered, relative to the control biofilm (Figure 3I). The derived Young's modulus of chloroquine-treated NTHI biofilms was significantly lower, compared to control biofilms (Figure 3J), which indicated that conversion of Z-DNA to B-DNA, destabilized the mechanical integrity of the biofilm. In contrast, NTHI biofilms incubated with DNase had a significantly higher Young's modulus, compared to control biofilms (Figure 3E). This latter result suggested that reduction of the proportion of B-DNA (e.g., via incubation with Pulmozyme), without affecting the steady-state levels of Z-DNA, increased the stiffness of the biofilm EPS.

Thus, according to our hypothesis, as Z-form DNA returns to B-form in the presence of chloroquine, this transformation should restore DNase susceptibility to the biofilm. To this end, NTHI biofilms (40 h) were incubated with chloroquine and/or DNase for 1 h. As shown in Figures 3K and S6A, there was a significant decrease in biofilm average thickness, which indicated that an equilibrium shift toward a B-DNA-dependent EPS transitioned the biofilm from a DNase-resistant to a DNase-sensitive state (Figure 3K). To determine whether this approach could be applied to clinical specimens, we obtained expectorated sputum samples from individuals with CF, which contain both a lattice of e-DNA and DNABII proteins (Novotny et al., 2013a). Sputa were culture-positive for *P. aeruginosa* (mucoid and non-mucoid) and *S. aureus* and all were resistant to specific antibiotics (Table S1). We employed a previously established sputum solids disruption assay (Gustave et al., 2013) to determine whether conversion of Z- to B-DNA increased susceptibility of CF sputum to DNase and/or chloroquine. To test this, we incubated sputum for 1 h with buffer, chloroquine (100 μM), DNase (30 U), or a combination of both, followed by optical density measurements to quantify the extent of disruption (Gustave et al., 2013). A representative image of the sputum solids disruption assay (Figure 3L) and the fold change of optical density (Figure 3M) demonstrated complete disruption of CF sputum solids when treated with both chloroquine and DNase. IF microscopy demonstrated that each clinical specimen contained both B- and Z-DNA (Figure S6B), organized within a distinct eDNA-rich lattice. Collectively, these data suggested that stable Z-DNA is the mode of DNase-resistance in the eDNA-dependent biofilm.

Resolution of extracellular HJs prevents Z-DNA formation in biofilms

We previously demonstrated, via the use of HJ-specific resolvases (RuvABC and RusA), that HJs are critical for the mechanical and structural stability of the eDNA lattice of bacterial biofilms (Devaraj et al., 2019). Here, we asked if the presence of HJs was also critical for Z-DNA stability. To test this, we allowed NTHI biofilms to form in the presence of RusA (10 μg/mL) for 16 h, then quantified the steady-state levels of both B-DNA and Z-DNA, as described above. The resolution of HJs by RusA markedly reduced the overall fluorescent intensity of bacterial biomass of the biofilm, with a concomitant reduction in the steady-state level of B-DNA, but nearly eliminated Z-DNA formation (Figures 4A–4D). These data suggested that maintenance of the HJ-like structures was critical for Z-DNA stability.

Exogenous DNABII proteins facilitate Z-DNA within biofilms

We reasoned that facilitation of biofilm development would have a specific kinetic threshold to which exogenous addition of HU would enhance Z-DNA accumulation. To test this, NTHI was incubated (and maintained) in the presence of HU_{NTHI} (100 nM) throughout biofilm development for 40 h. We performed IF for Z-DNA and found that an increased accumulation of Z-DNA was evident compared to the untreated control (Figures 4E–4G), which indicated that for NTHI, DNABII proteins are not limiting for biomass but continue to be required to modulate the equilibrium of the B-to-Z transition. Despite the fact that both $CeCl_3$ and DNABII require B-DNA as a reservoir to create stable Z-DNA, these agents likely achieve this outcome via different mechanisms.

Figure 4. Resolution of HJs prevent, whereas DNABII proteins facilitate, Z-DNA content within the biofilm

NTHI biofilms were initiated in the presence or absence of RusA (10 μg/mL) for 16 h at 37°C, then washed and incubated with rabbit monoclonal antibody against Z-DNA(Z22) (5 μg/mL) and a murine monoclonal antibody against B-DNA α-B-DNA(3519) (5 μg/mL), murine isotype IgG2a (Invitrogen, 02-6200), or IgG purified from unimmunized rabbit (5 μg/mL), then with goat α-rabbit IgG conjugated Alexa Fluor 405 (yellow) and goat α-mouse IgG conjugated Alexa Fluor 488 (cyan).

(A) Representative image of RusA prevention of Z-DNA.

(B–D) Signal intensities were quantified by ImageJ: (B) biomass (FM4-64 fluorescent signal), (C) B-DNA (Alexa Fluor 594), or (D) Z-DNA intensity (Alexa Fluor 488), n = 3.

(E) Representative image of NTHI biofilms that were initiated and maintained in the presence or absence of exogenous HU_{NTHI} (2 μg/mL) for 40 h at 37°C. Biofilms were then washed and incubated with rabbit monoclonal antibody against Z-DNA(Z22) (5 μg/mL) or IgG purified from unimmunized rabbit (5 μg/mL), then with goat α-rabbit IgG conjugated Alexa Fluor 488 (yellow).

(F and G) (F) Z-DNA intensity (Alexa Fluor 488) and (G) changes in biomass (FM4-64) were quantified by ImageJ, n = 3. To determine the mechanical properties of biofilms, NTHI biofilms were formed on fluorodishes and incubated with RusA or HU_{NTHI} as described above. Control experiments were performed, where HU_{NTHI} was added as described above, but was treated with Pulmozyme (50 μg/mL) or RusA (10 μg/mL) + Pulmozyme (50 μg/mL) for 1 h. Additionally, NTHI biofilms were grown for 24 h, incubated with $CeCl_3$ (500 μM) for 16 h, then treated with RusA (10 μg/mL) for 1 h at 37°C.

(H) Stress-strain curves were determined from axial mechanical indentation analysis.

(I) Young's modulus was determined from the lower linear region of the stress-strain curve (H), n = 3 (2 biofilms for each replicate were analyzed for a total of 6 biofilms per group). Statistical significance determined by one-way ANOVA and Dunnett's multiple comparison test. *p < 0.05, **p value ≤0.01, ***p value ≤ 0.001, and ****p value <0.0001; ns, not significant compared to control. Error bars represent the SEM.

See also Figure S5.

Z-DNA contributes to biofilm mechanical properties via HJs

To test whether HJ constraint stabilized Z-DNA in the EPS of bacterial biofilms, axial mechanical indentation was performed on control NTHI biofilms or those incubated with either a DNABII protein (HU_{NTHI}) or RusA, as described above. In addition, we added DNase for 1 h to biofilms incubated with HU_{NTHI} (throughout development), RusA (16 h), or a combination of both. Stress-strain analysis demonstrated that treatment with either protein altered the mechanical properties of the biofilm, compared to the control (Figure 4H). The Young's modulus for HU_{NTHI}-incubated biofilms was significantly greater than controls (Figure 4I). This indicated that increased Z-DNA in the biofilm, by interactions with a DNABII protein, led to significantly stiffer biofilms, similar to what was observed for $CeCl_3$-incubated biofilms (Figure 3E). Conversely, the Young's modulus of RusA-incubated biofilms was significantly less than controls (Figure 4I), which indicated that decreased Z-DNA destabilizes biofilm mechanical properties, similar to chloroquine treatment (Figure 3J). DNase did not alter the Young's modulus of either HU- or RusA-treated biofilms nor did HU alter the effect of RusA-treated biofilms. These results suggested that DNase has no additive or reductive effect on biofilm architecture once Z-DNA is either induced (via HJ stabilization by DNABII proteins) or resolved (via RusA). We demonstrated previously that HJs pre-bound with DNABII proteins are cleaved by RusA (Devaraj et al., 2019); thereby the failure of exogenous HU to mitigate RusA activity is expected. To provide further evidence that conversion of B to Z-DNA by $CeCl_3$ was dependent on eDNA, we incubated NTHI biofilms with $CeCl_3$ for 16 h, followed by incubation with RusA for 1 h. As shown, the Young's modulus was similar to RusA alone but reduced as compared to $CeCl_3$ alone (Figure 3E), i.e., the increased rigidity of $CeCl_3$-converted biofilms was completely abrogated by RusA (Figure 4I), which suggested that the increased rigidity by $CeCl_3$ was reliant on eDNA, and not due to other factors within the biofilm. Together, these results confirmed that extracellular HJs, mediated by DNABII proteins, contributed to the mechanical rigidity and structure of the biofilm via stabilization of Z-DNA.

DNABII proteins drive B-DNA dominant NETs to Z-DNA during PMA-induced NETosis

eDNA is ubiquitous in nature and a crucial structural component of multi-cellular communities (Ibáñez de Aldecoa et al., 2017). Although eubacteria release DNA *in vitro* (Ibáñez de Aldecoa et al., 2017; Jurcisek et al., 2017), biofilms within a host likely incorporate both bacterial and host-derived DNA (Alhede et al., 2020). Indeed, immune cells such as neutrophils release eDNA and associated antimicrobial compounds (e.g., histones) by NETosis (Dubois et al., 2012; Dwyer et al., 2014; Papayannopoulos et al., 2011) to control pathogens. This release of eukaryotic eDNA provides biofilm-resident bacteria an opportunity to incorporate both eukaryotic and bacterial-derived eDNA into their EPS. In this regard, there is a continuum of bacterial- and host-derived eDNA present at the site of infection (Alhede et al., 2020). Although it is expected that the interface between bacterial and host eDNA would vary in nucleoprotein complexes, we wondered whether DNABII proteins could, in and of themselves, also drive eukaryotic eDNA from its native B-form into the Z-form. First, we confirmed that neutrophils induced by phorbol-myristate-acetate (PMA) produced neutrophil extracellular traps (NETs) (Figures 5A, S7A, and S7B) and determined that the primary form of eDNA within PMA-induced NETs is B-DNA (Figures 5B and S7B). To recapitulate exposure to bacterial biofilms and their associated DNABII proteins, we added HU_{NTHI} to neutrophils at the time of PMA-induction. As demonstrated in Figure 5B, HU not only condensed the PMA-induced NETs, but converted a proportion of eDNA from B-form to Z-DNA. Conversely, CbpA, another minor groove DNA-binding protein (Chintakayala et al., 2015) also released by NTHI (Devaraj et al., 2018), failed to alter the appearance or proportion of B-form of the DNA (Figure S7B). Inactivation of NETs by DNase is well characterized and contributes to a loss of bacterial killing activity (Brinkmann et al., 2004; Mohanty et al., 2019), but whether a bacterial protein could mitigate bacterial killing is unknown. To test this hypothesis, we incubated neutrophils with DNase, HU_{NTHI}, CbpA, or buffer for 4 h with NTHI (16 h after seeding where the bacteria are in equilibrium between residence in the young biofilm and the planktonic state due to natural biofilm remodeling). Triton X-100 was added to lyse neutrophils to enable recovery of viable intracellular bacteria, and total CFU NTHI were enumerated for each condition to measure the relative percent bacterial killing within the system attributable to PMN NETosis (Robledo-Avila et al., 2020). As shown in Figure 5C, addition of either DNase or HU resulted in a marked reduction of measurable bacterial killing by NETs as compared to media control or CbpA. These collective results suggested that the proximity of DNABII proteins to host-derived eDNA not only could affect the form of eDNA, but also the ability of host cells to kill bacterial pathogens and/or control bacterial biofilm proliferation. We showed recently in a biofilm recovered from the middle ear of a chinchilla 11 days after challenge with NTHI (Devaraj et al., 2021) that host proteins (e.g., HMGB1) are localized near PMNs and PMN-derived eDNA, whereas DNABII proteins are primarily localized near the bacterial biofilm. However, at this host-pathogen interface, both proteins were visualized by IF. The ability of HMGB1 to disrupt bacterial biofilms (Devaraj et al., 2021) and the inactivation of NET-mediated bacterial killing function by DNABII proteins suggest a delicate balance at this interface. To now examine these regions within the same cryosections (Devaraj et al., 2021) for spatial distribution of B and Z-DNA, we observed a dense and extensive PMN-rich region located on and above the bacterial biofilm that is adhered to the middle ear mucosa (Figures 6A and 6B). The PMN-dense region contained both B-form and Z-form DNA within the eDNA lattice, however, the adherent NTHI biofilm was predominantly Z-DNA rich (Figures 6C–6E). Higher magnification insets Figure 6E provide further characterization and additional evidence of the localization of B-form and Z-form DNA within NETs. The uppermost portion above the biofilm within the middle ear lumen (e.g., recently migrated PMNs), contained predominantly B-DNA (Figure 6F). The top third "newer" region of the PMN-rich area (Figure 6G) contained both forms of DNA, whereas the bottom third "older" PMN region closest to the bacterial biofilm (Figure 6H) contained primarily Z-DNA. Z-DNA was the predominant form of eDNA within the bacterial biofilm adherent to the middle

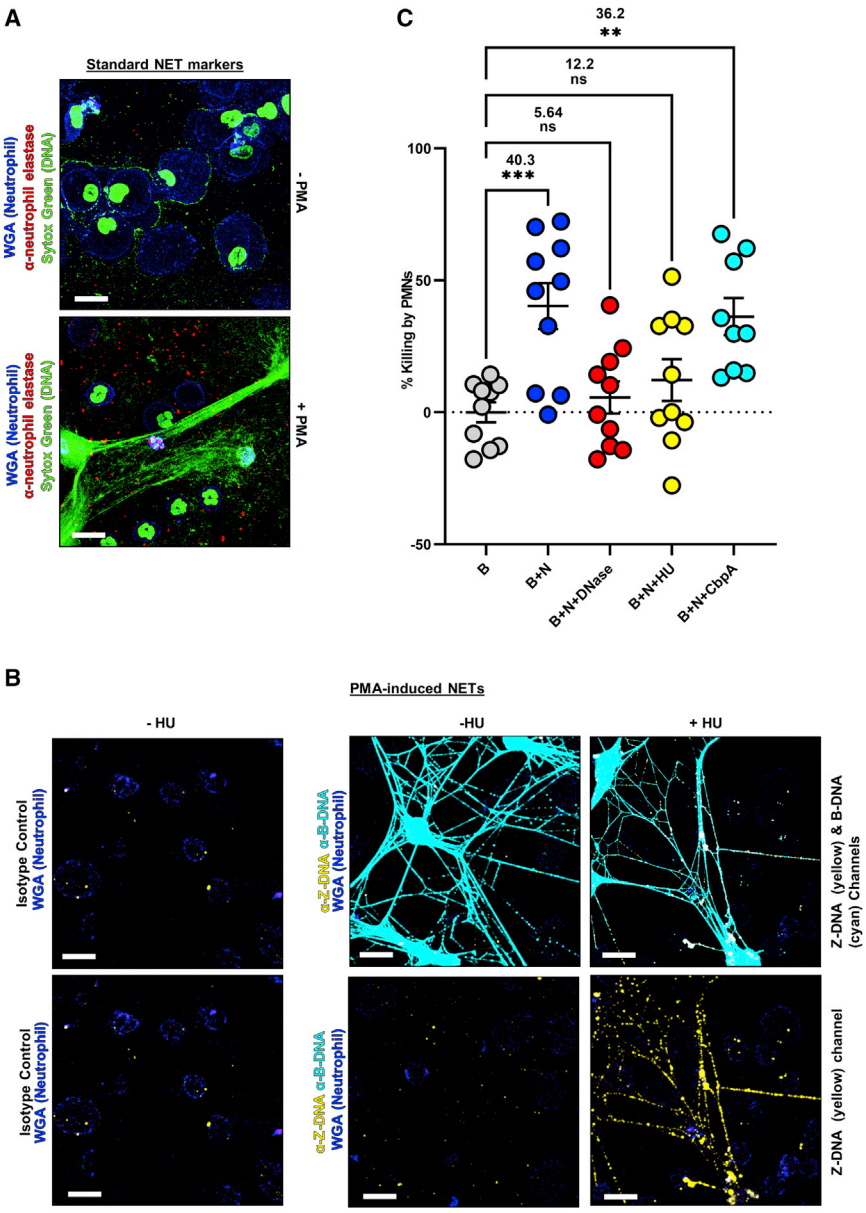

Figure 5. DNABII proteins inactivated NET function through the conversion of B-form NET eDNA to Z-form DNA

Neutrophils (1×10^5) were allowed to attach to an 8-well glass chamber slide and induced to NET with 200 nM PMA (phorbol-12-myristate-13-acetate) in the presence or absence of HU_{NTHI} (500 nM) for 3.5 h at 37°C. NETs were then fixed, washed, and blocked with 10% goat serum, followed by incubation with rabbit polyclonal antibody against human neutrophil elastase (1:100), rabbit monoclonal antibody against Z-DNA(Z22) (5 μg/mL), and a murine monoclonal antibody against B-DNA (5 μg/mL). Then NETs were incubated with goat α-rabbit IgG conjugated Alexa Fluor 594 and goat α-mouse IgG conjugated Alexa Fluor 488, wheat germ agglutinin (WGA 350), and SYTOX nucleic acid stain. NETs were imaged by CLSM.

(A) Representative images of NETs stained with the traditional NET markers, SYTOX (nucleic acid stain, green), neutrophil elastase (active NETs, red), and WGA (membrane stain, blue), n = 3.

(B) Representative images of NETs formed in the presence or absence of HU_{NTHI} demonstrated an increased Z-DNA signal only when exogenous DNABII proteins were added. Note that merged Z-DNA (yellow) and B-DNA (cyan) co-localize and appear white (n = 3).

(C) NETs killing is inactivated by DNABII proteins. NTHI biofilms were challenged with human neutrophils (B+N) and treated with 10 U/mL of Pulmozyme (B+N+Pulmo), 1 μM HU (B+N+HU), or 1 μM CbpA (B+N+CbpA) for 4 h. NTHI biofilm without neutrophils was used as a control (B). The bacteria challenged with neutrophils (B+N) (mean = 40.3%) and the group treated with CbpA (B+N+CbpA) (mean = 36.2%) showed a reduction in the relative % killing as compared to the biofilm control group (B). The bacteria treated with Pulmozyme (B+N+Pulmo) (mean = 5.64%) or with HU (B+N+HU) (mean = 12.2%) did not show differences in the relative % killing of bacteria by PMNs. The results suggest that Pulmozyme or HU treatment inactivated the NET function of bacterial killing. The graph plot replicates were derived from 4 healthy donors ± SEM. The statistical analysis was performed with one-way ANOVA and Dunnett's multiple comparison test (**$p < 0.01$, ***$p < 0.001$).

See also Figure S7.

ear mucosa (Figure 6I). Thus, because bacteria-released DNABII proteins accumulate not only within bacterial eDNA but also appeared to have migrated to NET-derived eDNA, where we hypothesize that conversion of NETs eDNA to Z-DNA could mitigate NET functions (e.g., bacterial killing), either through changes in NET structure and/or their capacity to maintain a high concentration gradient of antimicrobial molecules (e.g., histones which fail to bind Z-DNA) (Burton et al., 1978; Fishel et al., 1991; Nickol et al., 1982).

DISCUSSION

Since its discovery almost 50 years ago, Z-DNA has been exclusively characterized for its intracellular functions. In our present study, we revealed that extracellular Z-DNA provided a critical structural contribution and DNase-resistance to the eDNA-dependent EPS of bacterial biofilms.

Z-DNA provides multiple advantages over B-DNA as a biofilm matrix material. First, Z-DNA has a 3-fold greater persistence length compared to B-DNA and thereby can more effectively contribute to the structural integrity of the EPS. Second, we have argued that an underlying EPS for all bacteria that enter a multispecies biofilm would have great value to foster inclusion of diverse bacterial genera at large but exclude elements of potentially hazardous environments (Goodman et al., 2011). Because all eubacteria express DNA and DNABII proteins, all eubacteria produce the materials requisite for an inclusive EPS. The fact that it appears that a biofilm structure inclusive

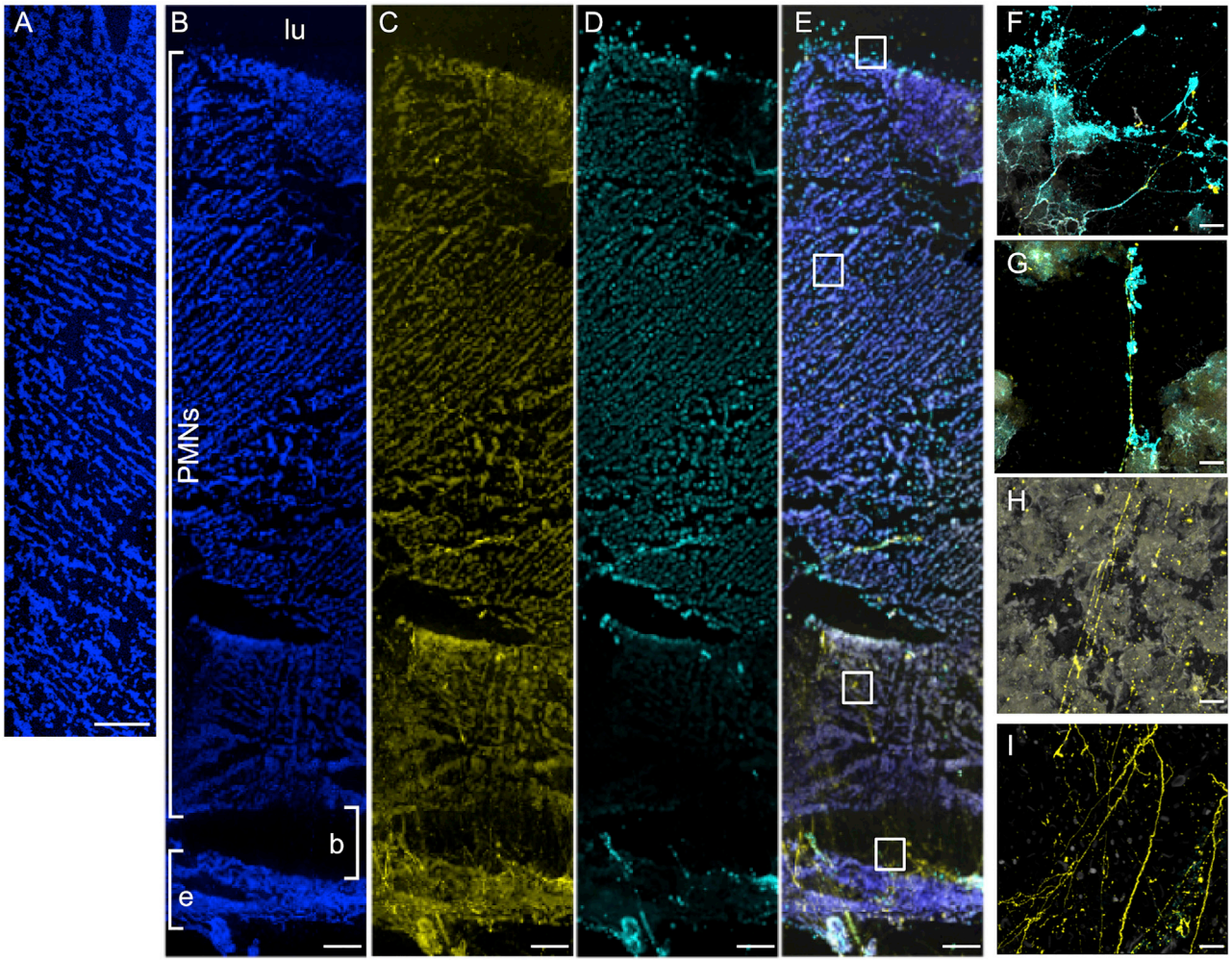

Figure 6. Tiled CSLM images of an immunolabeled biofilm recovered from the middle ear of a chinchilla 11 days after challenge with NTHI

The cryosection was labeled with (A) isotype control rabbit serum and isotype control mouse serum + Alexa Fluor 594-conjugated goat α-rabbit serum and Alexa Fluor 488-conjugated goat α-mouse serum respectively; (B) DAPI to identify ds-DNA; (C) rabbit α-Z-DNA + Alexa Fluor 594-conjugated goat α-rabbit serum (pseudocolored yellow); and (D) murine anti-B-DNA + Alexa Fluor 488-conjugated goat α-mouse serum (pseudocolored cyan).

(E) Composite image of overlaid (B)–(D).

(F–I) Higher magnification 3D reconstructions of z stack images taken from the portions of the biomass as indicated by the boxed regions in (E).

(F) The uppermost portion of the biofilm closest to the lumen of the middle ear where the most recently migrated PMNs are located.

(G) Top third of the PMN-rich region of this cryosection.

(H) Bottom third of the PMN-rich region.

(I) Bacterial biofilm.

Note that dsDNA is present throughout this cryosection as evidenced by DAPI labeling in (B), however, it is only in B-form in the PMN-rich region and not within the bacterial biofilm, as evidence by (D). Conversely, DNA in the bacterial biofilm is in Z-form as evidenced by labeling visible in (C) but absent in (D). Labeling within insets provide additional evidence for the B-form DNA that predominates in the NETs formed by the most recently migrated PMNs (F); strands of DNA labeled for both B- and Z-form DNA in PMN-rich regions that are "older" (e.g., within the middle region of the cryosection) (G); exclusively Z-form DNA labeling of NETs formed by PMNs closest to the bacterial biofilm (H); and exclusively Z-form of the eDNA within the bacterial biofilm that is adherent to the middle ear mucosa (I). Scale bars, 200 μm (A–E) and 5 μm (F–I). To best resolve deep blue DAPI labeling against the black background in (A) and (B), the brightness of these two panels only was increased. lu, lumen of the middle ear; PMNs, dense extensive PMN-rich region above the bacterial biofilm; b, NTHI biofilm adherent to the middle ear mucosa; e, epithelium that lines the middle ear space.

of Z-DNA is also conserved provides additional evidence in support of this model. Third, an underlying Z-DNA-dependent EPS is highly resistant to DNA nucleases. It is well known that various pathogens secrete nucleases to release themselves from the B form-eDNA tendrils released by NETs, likely a critical step in pathogen dispersal and propagation from the biofilm reservoir (Storisteanu et al., 2017; Tran et al., 2016). With the eDNA of bacterial biofilms in the Z-form, and the NETs eDNA initially in the B-form, secreted nucleases would allow bacteria to leave biofilm residence without the danger of NET-mediated killing, as evidenced by the likelihood of DNABII-mediated inactivation. Finally, nearly all DNA-binding proteins bind to B-form DNA but

not to Z-DNA. Indeed, the potent antimicrobial activity of NET-released histone is reliant upon histones being in the bound state that effectively concentrates their antimicrobial activity within this B-form eDNA NET (Brinkmann et al., 2004). Given that DNABII proteins are likely the rate limiting effector to drive NET eDNA into the Z-form, it has not escaped our attention that any eDNA (e.g., that deployed by NETs) within the effective diffusion radius of the bacterial biofilm EPS could be subject to conversion to the Z-form. When active on NET-deployed eDNA, this would induce histones into an unbound state, and thus a loss of their concentration gradient and effectiveness against targeted biofilms. The effective failure of localized histone-mediated antimicrobial activity would be a strong immune evasion mechanism for biofilm-resident bacteria. Moreover, histones are cytotoxic (Singh et al., 2010), and thus histones released from NETs by conversion to Z-form have the potential to inadvertently cause collateral damage to host tissues.

How does Z-DNA form within the biofilm EPS? B- and Z-form DNA (regardless of sequence) (Kypr et al., 2009) are in equilibrium (Guéron et al., 2000; Lee et al., 2018; Zacharias et al., 1988), with the B-form dominating under physiologic conditions. Although the equilibrium shift from B to Z can readily be induced (Ali and Ali, 1997; Bhanjadeo et al., 2017; Thomas and Messner, 1988; Zhang et al., 2019), these conditions do not typically occur in native systems due to the high intrinsic energy requirement of Z-DNA (Dumat et al., 2016; Ho et al., 1991; Kim et al., 2018). Our results show a system with, and dependent on, development of a stable Z-DNA state that increases in magnitude with biofilm maturity. Indeed, $CeCl_3$, a known catalyst of Z-DNA formation, increased both the magnitude of the biomass and the Z-DNA content of the biofilm. In addition, DNase treatment of mature biofilms that reduces the proportion of B-DNA but does not affect the extant steady-state levels of Z-DNA, also stiffened biofilm structure. This outcome indicated that the presence of some B-DNA makes biofilms less stiff and hence more flexible, a property that may be important during the life cycle of the biofilm. In contrast, chloroquine, a known intercalator of B-DNA that drives Z-DNA back into the B-DNA state, reduced both the magnitude of the biomass and Z-DNA content of the biofilm. Interestingly, addition of DNABII proteins has an effect that is similar, but not identical, to $CeCl_3$ addition. According to our model, under native conditions, the equilibrium state of DNA is predominantly in the B-form. The presence of endogenous extracellular DNABII proteins constrains more of the eDNA in the Z-form, which stabilizes the eDNA-dependent EPS (Figures 7A–7C, top panel). When $CeCl_3$ is added, the equilibrium shift toward production of Z-DNA is increased, which drives a greater proportion of eDNA into the Z-form (Figure 7D, top panel). In contrast, when chloroquine is added the equilibrium shift that drives DNA into the B-form is increased, which favors disassembly of the eDNA-dependent EPS (Figure 7E. top panel). When exogenous DNABII is added, the equilibrium shift favors more eDNA in the Z-form (Figure 7F, top panel). Although DNABII proteins bind various DNA substrates (Bonnefoy and Rouvière-Yaniv, 1991; Kamashev and Rouviere-Yaniv, 2000; Rice et al., 1996; Swinger and Rice, 2004, 2007), there is no direct evidence that DNABII proteins bind Z-DNA, thus we posit that they instead constrain and stabilize the Z-DNA (Bae et al., 2011) configuration via HJ-like structures. Indeed, in the solved IHF co-crystal with DNA, the terminal nucleotides in the complex are in the *anti-syn* conformation indicative of Z-DNA (Rice et al., 1996; Zhou et al., 2019). Thus, in this context, HJs are conduits for both B- and Z-form DNA. Per our proposed model, B-form predominates when linear ds-DNA has free ends, and the DNABII proteins are in equilibrium between HJ-bound and linear DNA-bound (Figure 7A, bottom panel) wherein the dsDNA is wrapped or twisted around DNABII proteins (a known property of at least HU proteins). As the DNABII proteins migrate to stabilize HJs and a closed loop is formed (Figure 7B, bottom panel), the ends of DNA could be locked in a high energy state (e.g., where the twist vacated by the DNABII proteins is converted to supercoiling) conducive for Z-DNA formation (Nordheim and Rich, 1983; Thomas and Messner, 1988; Wittig et al., 1991), with as few as 3 HJs that serve to constrain three strands of dsDNA (Figure 7C, bottom panel) and only utilize 2 of 4 arms of each HJ. The remaining arms would act as conduits to the B-DNA reservoir. In agreement with this model, if there is a sufficient steady-state level of DNABII proteins to stabilize the HJs, the configuration is locked, and as a consequence, the B-form DNA-binding DNABII proteins can no longer bind the intervening sequences as they are in a Z-configuration (Figures 7D and 7E, bottom panels).

This model is also consistent with several of our observations. First, when chloroquine binds dsDNA, it unwinds the DNA, thus absorbing the writhe that DNABII proteins create when migrated to the HJs, thereby reverting Z-DNA back into B-form. Second, because $CeCl_3$ promotes Z-DNA formation, it would act as an additional stimulatory factor in the transition from supercoiling (Figure 7C, bottom panel) to "flipping" into Z-DNA (Figure 7D, bottom panel). Indeed, this may indicate that other naturally occurring cations (e.g., polyamines) could also facilitate the stabilization of Z-DNA (Thomas and Messner, 1988; Thomas et al., 1991). Third, cleavage of the HJs would release the ends of the dsDNA allowing free rotation of the DNA ends with an equilibrium shift back to B-form DNA and concomitant collapse of the biofilm matrix eDNA-rich structure. Interestingly, others have shown the reverse phenomenon with similar, yet synthetic structures. When B-form DNA is locked into a 2D array of HJs (DNA origami) (Shrestha et al., 2016) such that the ends are not free to rotate, conditions that otherwise favor Z-DNA cannot facilitate the transition from B-DNA (Rajendran et al., 2013). Although the exact mechanism of lattice formation awaits future studies, only when the HJ-like structures within the biofilm EPS are present is Z-DNA observed.

Whether the host immune system directly reconciles an abundance of Z-DNA in the EPS of bacterial biofilms has yet to be shown, although there is ample evidence for the involvement of Z-DNA-binding proteins in the innate immune response and host-pathogen interactions (Feng et al., 2011; Kim et al., 2003; Kwon and Rich, 2005; Oh et al., 2002; Ray et al., 2013; Shin et al., 2016; Szczesny et al., 2018; van der Vorst et al., 2018; Wang et al., 2006; Zavarykina et al., 2019). We propose that bacterial-derived Z-DNA within biofilms is a major contributor to the reservoir of Z-DNA within the host. Z-DNA is more antigenic than B-DNA (Möller et al., 1982; Rich and Zhang, 2003), and antibodies specific to Z-DNA are more abundant in autoimmune diseases, in particular SLE (Rich and Zhang, 2003) and rheumatoid

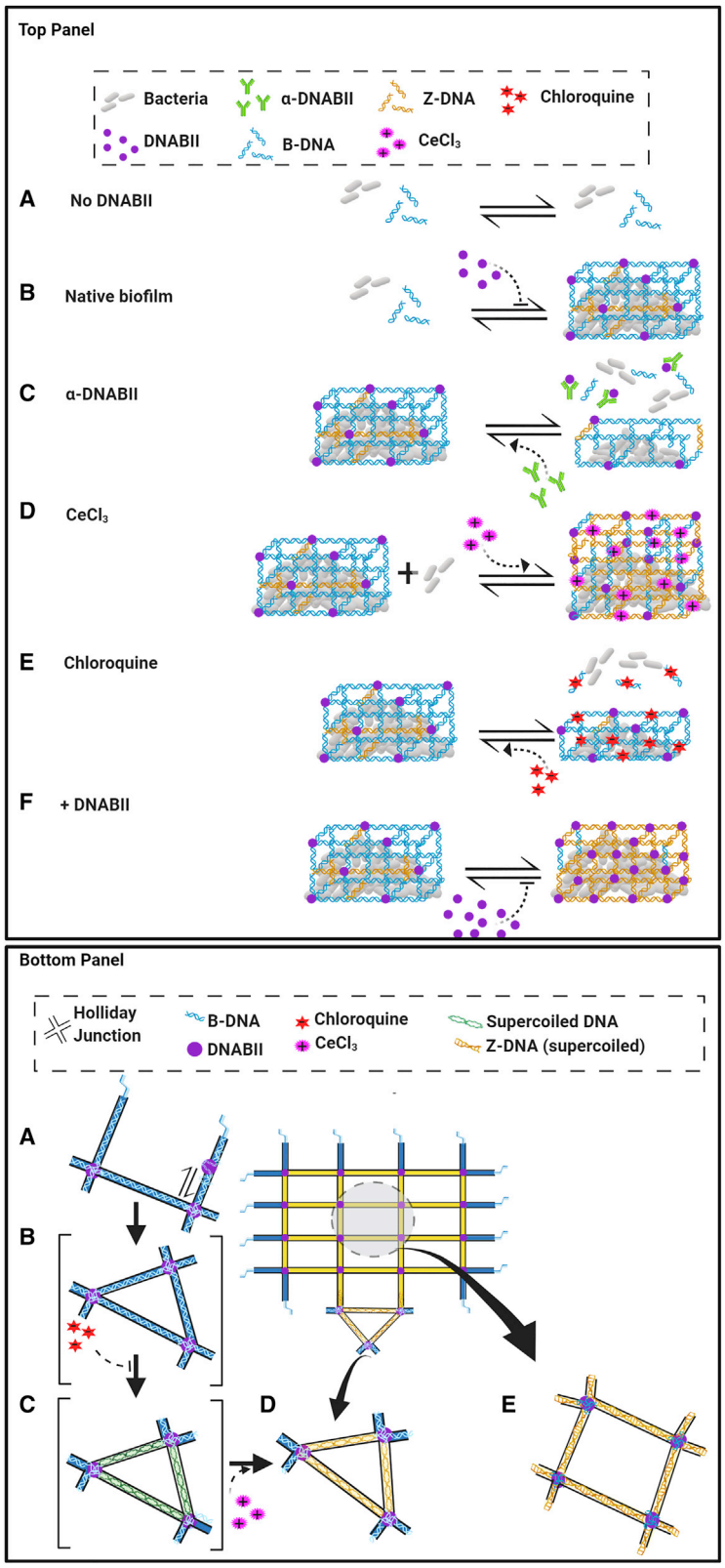

Figure 7. Models of the B/Z-DNA equilibrium and the HJ constrained eDNA of the biofilm

Top panel: (A) In the absence of DNABII proteins, there is no eDNA lattice structure. (B) In the presence of DNABII proteins, native biofilm the equilibrium shifts between B-form and Z-form eDNA. (C) Antibodies directed against DNABII proteins collapse bacterial biofilms as this favors B-form eDNA. (D) $CeCl_3$ favors Z-form eDNA, which stabilizes the biofilm matrix and promotes biofilm residence. (E) Chloroquine favors B-form eDNA, which destabilizes the biofilm matrix and releases bacteria from biofilm residence. (F) Exogenous DNABII proteins shift the equilibrium to favor Z-DNA via Holliday junction-like stabilization.

Bottom panel: (A) B-form predominates when linear dsDNA has free ends, and the DNABII proteins are in equilibrium between HJ-bound and linear DNA-bound. (B) DNABII proteins migrate to stabilize HJs and a closed loop is formed. (C) The ends of DNA could be locked in a high energy state (>3 HJs). The transition from (B) to (C) is inhibited by chloroquine, whereas the $CeCl_3$ stimulates the transition from (C) to (D) (e.g., supercoiling "flips" to Z-form. (D) Z-DNA is constrained. (E) Z-DNA is stabilized within the ds-DNA matrix (4HJs).

arthritis (RA) (Sibley et al., 1984). Individuals with SLE or RA also have a higher prevalence of bacterial infections (Bouza et al., 2001). This clinical outcome may be the result of host-derived Z-DNA-binding proteins, or the induction of Z-DNA-specific antibodies during the course of these chronic diseases that inadvertently stabilizes the bacterial biofilm EPS. We also propose that bacterial DNABII proteins facilitate B-to Z-DNA conversion of NET-deployed eDNA at the site of bacterial biofilm-mediated disease, which mitigates the action of host immune effectors. Based on our model, we propose that DNABII interaction with host eDNA results in a three-pronged effect. First, it would permit bacteria to utilize the reservoir of NET eDNA for biofilm development. Second, any antimicrobial B-form DNA-binding proteins (e.g., histones) would lose their affinity for the NET-derived eDNA because it is converted into the Z-form. Finally, it is also possible that bacterial infections are part of a cycle, where the adaptive immune response produces Z-DNA-specific antibodies in response to biofilm infections, which inadvertently results in increased initiation and durability of bacterial biofilm formation as mediated by stabilization of a Z-DNA-rich structure (Moinuddin et al., 1998), reduces the threshold of conditions needed for Z-DNA induction (Lafer et al., 1985), and ultimately promotes chronic infection. Taken together, the role of Z-DNA in the structural stability of bacterial biofilms could be part of a much larger signal recognition response by the host innate immune system to detect foreign DNA, a hierarchical transition from rare DNA structure with an uncharacterized cellular role to a central component in the innate immune response. The development and use of therapeutic agents designed to drive biofilm eDNA back into its native B-form could provide additional approaches for clinical resolution, or prevention, of biofilm-mediated diseases.

Limitations of study

Despite strong evidence that supports a structural role of Z-DNA in the eDNA-dependent EPS of bacterial biofilms, there are two limitations to this study. First, although the antibodies we used that were directed against B or Z DNA are highly specific, their overall access to each form of DNA substrate within the biofilm matrix could be variable and dependent upon the overall structure and/or constituents of the biofilm. If true, this result would not affect our overall conclusions, and instead would speak to the relative contributions of B-DNA and Z-DNA to biofilm structure. Second, although our data strongly supports DNA, DNABII proteins, and Z-DNA as necessary components of the eDNA-dependent matrix, we cannot rule out that these components are insufficient to recapitulate the native biofilm structure; other universally available biofilm components may be required. Future experiments will focus on determining the fine structure of this extracellular nucleoprotein matrix to further dissect the apparent underlying architecture common to bacterial biofilms.

STAR★METHODS

Detailed methods are provided in the online version of this paper and include the following:

- KEY RESOURCES TABLE
- RESOURCE AVAILABILITY
  - Lead contact
  - Materials availability
  - Data and code availability
- EXPERIMENTAL MODEL AND SUBJECT DETAILS
  - Bacterial strains
  - Human-derived samples
  - Chinchilla model
- METHOD DETAILS
  - Bacterial growth
  - *In vitro* biofilms
  - Antibodies
  - Nuclease resistance of biofilms
  - Antibody specificity of B- and Z-DNA antibodies
  - Pulmozyme protection assay
  - Verification of antibody cross-reactivity by western blot
  - B-DNA and Z-DNA increases during biofilm maturation
  - Visualization of B-DNA and Z-DNA in biofilms formed *in vitro*
  - Visualization of B-DNA and Z-DNA in biofilms formed on HAEs
  - Visualization of B-DNA and Z-DNA within clinical specimens
  - Quantification of Z-DNA and B-DNA within nuclease-treated biofilms
  - Stimulation of biofilm formation by anti-Z-DNA
  - Confirmation of B/Z-DNA conversion by OD 260/295
  - Growth curves of planktonic NTHI
  - Modulation of B/Z eDNA of bacterial biofilms
  - Axial mechanical indentation of NTHI biofilms
  - The susceptibility of biofilms to DNase after chloroquine
  - The susceptibility of clinical specimens to DNase and chloroquine
  - Prevention of Z-DNA formation by a HJ resolvase
  - DNABII proteins drive B-DNA dominant NETs to Z-DNA during PMA-induced NETosis
  - NET inactivation of bacterial killing
  - Image of 11 day challenged chinchilla sections
- QUANTIFICATION AND STATISTICAL ANALYSIS

SUPPLEMENTAL INFORMATION

Supplemental information can be found online at https://doi.org/10.1016/j.cell.2021.10.010.

ACKNOWLEDGMENTS

We thank Jeffrey Melvin, PhD, for thoughtful discussions. We also thank the C3 Epithelial Cell Core at Nationwide Children's Hospital which is supported by a research development grant from the Cystic Fibrosis Foundation. Finally, we extend our gratitude to those individuals who donated CF sputum samples through IRB11-00790 that was approved by the Nationwide Children's Hospital Institutional Review Board. This work was supported by NIH (R01DC 011818 and R01AI155501 to S.D.G. and L.O.B. and R01GM124436 to P.S.).

AUTHOR CONTRIBUTIONS

J.R.B., A.D., L.O.B., and S.D.G. designed the research. J.R.B., A.D., E.S.G., L.M.-W., F.R.-A., T.K., K.W., S.B., J.W., and L.A.N performed the research. F.R.-A. and J.A.J contributed new reagents and/or analytic tools. J.R.B.,

A.D., E.S.G., L.M.-W., F.R.-A., L.A.N., P.S., L.O.B., and S.D.G. analyzed the data. J.R.B., E.S.G., L.O.B., and S.D.G. wrote the paper.

DECLARATION OF INTERESTS

S.D.G. and L.O.B. are founders, shareholders, and members of the scientific advisory board of Clarametyx Biosciences, Inc.

Received: January 22, 2021
Revised: August 3, 2021
Accepted: October 12, 2021
Published: November 3, 2021

REFERENCES

Al-Bari, M.A. (2015). Chloroquine analogues in drug discovery: new directions of uses, mechanisms of actions and toxic manifestations from malaria to multifarious diseases. J. Antimicrob. Chemother. *70*, 1608–1621.

Alhede, M., Alhede, M., Qvortrup, K., Kragh, K.N., Jensen, P.O., Stewart, P.S., and Bjarnsholt, T. (2020). The origin of extracellular DNA in bacterial biofilm infections in vivo. Pathog. Dis. *78*, ftaa018.

Ali, N., and Ali, R. (1997). High salt and solvent induced Z-conformation in native calf thymus DNA. Biochem. Mol. Biol. Int. *41*, 1227–1235.

Bae, S., Kim, D., Kim, K.K., Kim, Y.G., and Hohng, S. (2011). Intrinsic Z-DNA is stabilized by the conformational selection mechanism of Z-DNA-binding proteins. J. Am. Chem. Soc. *133*, 668–671.

Baranovskii, A.G., Buneva, V.N., and Nevinsky, G.A. (2004). Human deoxyribonucleases. Biochemistry (Mosc.) *69*, 587–601.

Bezanilla, M., Drake, B., Nudler, E., Kashlev, M., Hansma, P.K., and Hansma, H.G. (1994). Motion and enzymatic degradation of DNA in the atomic force microscope. Biophys. J. *67*, 2454–2459.

Bhanjadeo, M.M., Nayak, A.K., and Subudhi, U. (2017). Cerium chloride stimulated controlled conversion of B-to-Z DNA in self-assembled nanostructures. Biochem. Biophys. Res. Commun. *482*, 916–921.

Bonnefoy, E., and Rouvière-Yaniv, J. (1991). HU and IHF, two homologous histone-like proteins of Escherichia coli, form different protein-DNA complexes with short DNA fragments. EMBO J. *10*, 687–696.

Bouza, E., Moya, J.G., and Muñoz, P. (2001). Infections in systemic lupus erythematosus and rheumatoid arthritis. Infect. Dis. Clin. North Am. *15*, 335–361, vii.

Brinkmann, V., Reichard, U., Goosmann, C., Fauler, B., Uhlemann, Y., Weiss, D.S., Weinrauch, Y., and Zychlinsky, A. (2004). Neutrophil extracellular traps kill bacteria. Science *303*, 1532–1535.

Brockson, M.E., Novotny, L.A., Mokrzan, E.M., Malhotra, S., Jurcisek, J.A., Akbar, R., Devaraj, A., Goodman, S.D., and Bakaletz, L.O. (2014). Evaluation of the kinetics and mechanism of action of anti-integration host factor-mediated disruption of bacterial biofilms. Mol. Microbiol. *93*, 1246–1258.

Burton, D.R., Butler, M.J., Hyde, J.E., Phillips, D., Skidmore, C.J., and Walker, I.O. (1978). The interaction of core histones with DNA: equilibrium binding studies. Nucleic Acids Res. *5*, 3643–3663.

Chaires, J.B. (1983). Daunomycin inhibits the B leads to Z transition in poly d(G-C). Nucleic Acids Res. *11*, 8485–8494.

Chaires, J.B., and Norcum, M.T. (1988). Structure and stability of Z* DNA. J. Biomol. Struct. Dyn. *5*, 1187–1207.

Chintakayala, K., Sellars, L.E., Singh, S.S., Shahapure, R., Westerlaken, I., Meyer, A.S., Dame, R.T., and Grainger, D.C. (2015). DNA recognition by Escherichia coli CbpA protein requires a conserved arginine-minor-groove interaction. Nucleic Acids Res. *43*, 2282–2292.

Devaraj, A., Justice, S.S., Bakaletz, L.O., and Goodman, S.D. (2015). DNABII proteins play a central role in UPEC biofilm structure. Mol. Microbiol. *96*, 1119–1135.

Devaraj, A., Buzzo, J., Rocco, C.J., Bakaletz, L.O., and Goodman, S.D. (2018). The DNABII family of proteins is comprised of the only nucleoid associated proteins required for nontypeable Haemophilus influenzae biofilm structure. MicrobiologyOpen *7*, e00563.

Devaraj, A., Buzzo, J.R., Mashburn-Warren, L., Gloag, E.S., Novotny, L.A., Stoodley, P., Bakaletz, L.O., and Goodman, S.D. (2019). The extracellular DNA lattice of bacterial biofilms is structurally related to Holliday junction recombination intermediates. Proc. Natl. Acad. Sci. USA *116*, 25068–25077.

Devaraj, A., Novotny, L.A., Robledo-Avila, F.H., Buzzo, J.R., Mashburn-Warren, L., Jurcisek, J.A., Tjokro, N.O., Partida-Sanchez, S., Bakaletz, L.O., and Goodman, S.D. (2021). The extracellular innate-immune effector HMGB1 limits pathogenic bacterial biofilm proliferation. J. Clin. Invest. *131*, e140527.

Dey, D., Nagaraja, V., and Ramakumar, S. (2017). Structural and evolutionary analyses reveal determinants of DNA binding specificities of nucleoid-associated proteins HU and IHF. Mol. Phylogenet. Evol. *107*, 356–366.

Dubois, A.V., Gauthier, A., Bréa, D., Varaigne, F., Diot, P., Gauthier, F., and Attucci, S. (2012). Influence of DNA on the activities and inhibition of neutrophil serine proteases in cystic fibrosis sputum. Am. J. Respir. Cell Mol. Biol. *47*, 80–86.

Dumat, B., Larsen, A.F., and Wilhelmsson, L.M. (2016). Studying Z-DNA and B- to Z-DNA transitions using a cytosine analogue FRET-pair. Nucleic Acids Res. *44*, e101.

Dwyer, M., Shan, Q., D'Ortona, S., Maurer, R., Mitchell, R., Olesen, H., Thiel, S., Huebner, J., and Gadjeva, M. (2014). Cystic fibrosis sputum DNA has NETosis characteristics and neutrophil extracellular trap release is regulated by macrophage migration-inhibitory factor. J. Innate Immun. *6*, 765–779.

Edgington, S.M., and Stollar, B.D. (1992). Immunogenicity of Z-DNA depends on the size of polynucleotide presented in complexes with methylated BSA. Mol. Immunol. *29*, 609–617.

Feng, S., Li, H., Zhao, J., Pervushin, K., Lowenhaupt, K., Schwartz, T.U., and Dröge, P. (2011). Alternate rRNA secondary structures as regulators of translation. Nat. Struct. Mol. Biol. *18*, 169–176.

Fishel, R., Derbyshire, M.K., Moore, S.P., and Young, C.S.H. (1991). Biochemical studies of homologous and nonhomologous recombination in human cells. Biochimie *73*, 257–267.

Flemming, H.C., and Wingender, J. (2010). The biofilm matrix. Nat. Rev. Microbiol. *8*, 623–633.

Frederiksen, B., Pressler, T., Hansen, A., Koch, C., and Høiby, N. (2006). Effect of aerosolized rhDNase (Pulmozyme) on pulmonary colonization in patients with cystic fibrosis. Acta Paediatr. *95*, 1070–1074.

Gloag, E.S., German, G.K., Stoodley, P., and Wozniak, D.J. (2018). Viscoelastic properties of Pseudomonas aeruginosa variant biofilms. Sci. Rep. *8*, 9691.

Goodman, S.D., Obergfell, K.P., Jurcisek, J.A., Novotny, L.A., Downey, J.S., Ayala, E.A., Tjokro, N., Li, B., Justice, S.S., and Bakaletz, L.O. (2011). Biofilms can be dispersed by focusing the immune system on a common family of bacterial nucleoid-associated proteins. Mucosal Immunol. *4*, 625–637.

Grove, A. (2011). Functional evolution of bacterial histone-like HU proteins. Curr. Issues Mol. Biol. *13*, 1–12.

Guéron, M., Demaret, J., and Filoche, M. (2000). A unified theory of the B-Z transition of DNA in high and low concentrations of multivalent ions. Biophys. J. *78*, 1070–1083.

Gunn, J.S., Bakaletz, L.O., and Wozniak, D.J. (2016). What's on the Outside Matters: The Role of the Extracellular Polymeric Substance of Gram-negative Biofilms in Evading Host Immunity and as a Target for Therapeutic Intervention. J. Biol. Chem. *291*, 12538–12546.

Gustave, J.E., Jurcisek, J.A., McCoy, K.S., Goodman, S.D., and Bakaletz, L.O. (2013). Targeting bacterial integration host factor to disrupt biofilms associated with cystic fibrosis. J. Cyst. Fibros. *12*, 384–389.

Hall-Stoodley, L., Nistico, L., Sambanthamoorthy, K., Dice, B., Nguyen, D., Mershon, W.J., Johnson, C., Hu, F.Z., Stoodley, P., Ehrlich, G.D., and Post, J.C. (2008). Characterization of biofilm matrix, degradation by DNase treatment and evidence of capsule downregulation in Streptococcus pneumoniae clinical isolates. BMC Microbiol. *8*, 173.

Harrison, A., Dyer, D.W., Gillaspy, A., Ray, W.C., Mungur, R., Carson, M.B., Zhong, H., Gipson, J., Gipson, M., Johnson, L.S., et al. (2005). Genomic sequence of an otitis media isolate of nontypeable Haemophilus influenzae: comparative study with H. influenzae serotype d, strain KW20. J. Bacteriol. *187*, 4627–4636.

Heegaard, N.H.H., Olsen, D.T., and Larsen, K.-L.P. (1996). Immuno-capillary electrophoresis for the characterization of a monoclonal antibody against DNA. J. Chromatogr. A *744*, 285–294.

Heydorn, A., Nielsen, A.T., Hentzer, M., Sternberg, C., Givskov, M., Ersbøll, B.K., and Molin, S. (2000). Quantification of biofilm structures by the novel computer program COMSTAT. Microbiology (Reading) *146*, 2395–2407.

Ho, P.S., Kagawa, T.F., Tseng, K.H., Schroth, G.P., and Zhou, G.W. (1991). Prediction of a crystallization pathway for Z-DNA hexanucleotides. Science *254*, 1003–1006.

Ibáñez de Aldecoa, A.L., Zafra, O., and González-Pastor, J.E. (2017). Mechanisms and Regulation of Extracellular DNA Release and Its Biological Roles in Microbial Communities. Front. Microbiol. *8*, 1390.

Jurcisek, J.A., and Bakaletz, L.O. (2007). Biofilms formed by nontypeable Haemophilus influenzae in vivo contain both double-stranded DNA and type IV pilin protein. J. Bacteriol. *189*, 3868–3875.

Jurcisek, J.A., Brockman, K.L., Novotny, L.A., Goodman, S.D., and Bakaletz, L.O. (2017). Nontypeable *Haemophilus influenzae* releases DNA and DNABII proteins via a T4SS-like complex and ComE of the type IV pilus machinery. Proc. Natl. Acad. Sci. USA *114*, E6632–E6641.

Kamashev, D., and Rouviere-Yaniv, J. (2000). The histone-like protein HU binds specifically to DNA recombination and repair intermediates. EMBO J. *19*, 6527–6535.

Kaplan, J.B., LoVetri, K., Cardona, S.T., Madhyastha, S., Sadovskaya, I., Jabbouri, S., and Izano, E.A. (2012). Recombinant human DNase I decreases biofilm and increases antimicrobial susceptibility in staphylococci. J. Antibiot. (Tokyo) *65*, 73–77.

Kassinger, S.J., and van Hoek, M.L. (2020). Biofilm architecture: An emerging synthetic biology target. Synth. Syst. Biotechnol. *5*, 1–10.

Kim, Y.G., Lowenhaupt, K., Maas, S., Herbert, A., Schwartz, T., and Rich, A. (2000). The zab domain of the human RNA editing enzyme ADAR1 recognizes Z-DNA when surrounded by B-DNA. J. Biol. Chem. *275*, 26828–26833.

Kim, Y.G., Muralinath, M., Brandt, T., Pearcy, M., Hauns, K., Lowenhaupt, K., Jacobs, B.L., and Rich, A. (2003). A role for Z-DNA binding in vaccinia virus pathogenesis. Proc. Natl. Acad. Sci. USA *100*, 6974–6979.

Kim, S.H., Lim, S.H., Lee, A.R., Kwon, D.H., Song, H.K., Lee, J.H., Cho, M., Johner, A., Lee, N.K., and Hong, S.C. (2018). Unveiling the pathway to Z-DNA in the protein-induced B-Z transition. Nucleic Acids Res. *46*, 4129–4137.

Koo, H., Allan, R.N., Howlin, R.P., Stoodley, P., and Hall-Stoodley, L. (2017). Targeting microbial biofilms: current and prospective therapeutic strategies. Nat. Rev. Microbiol. *15*, 740–755.

Kuriakose, T., and Kanneganti, T.D. (2018). ZBP1: Innate Sensor Regulating Cell Death and Inflammation. Trends Immunol. *39*, 123–134.

Kwakye-Berko, F., and Meshnick, S. (1990). Sequence preference of chloroquine binding to DNA and prevention of Z-DNA formation. Mol. Biochem. Parasitol. *39*, 275–278.

Kwon, J.A., and Rich, A. (2005). Biological function of the vaccinia virus Z-DNA-binding protein E3L: gene transactivation and antiapoptotic activity in HeLa cells. Proc. Natl. Acad. Sci. USA *102*, 12759–12764.

Kypr, J., Kejnovská, I., Renciuk, D., and Vorlícková, M. (2009). Circular dichroism and conformational polymorphism of DNA. Nucleic Acids Res. *37*, 1713–1725.

Lafer, E.M., Sousa, R., and Rich, A. (1985). Anti-Z-DNA antibody binding can stabilize Z-DNA in relaxed and linear plasmids under physiological conditions. EMBO J. *4* (13B), 3655–3660.

Lafer, E.M., Sousa, R., Ali, R., Rich, A., and Stollar, B.D. (1986). The effect of anti-Z-DNA antibodies on the B-DNA-Z-DNA equilibrium. J. Biol. Chem. *261*, 6438–6443.

Lee, A.R., Kim, N.H., Seo, Y.J., Choi, S.R., and Lee, J.H. (2018). Thermodynamic Model for B-Z Transition of DNA Induced by Z-DNA Binding Proteins. Molecules *23*, 2748.

Mangan, M.W., Lucchini, S., Danino, V., Cróinín, T.O., Hinton, J.C., and Dorman, C.J. (2006). The integration host factor (IHF) integrates stationary-phase and virulence gene expression in Salmonella enterica serovar Typhimurium. Mol. Microbiol. *59*, 1831–1847.

Martins, M., Henriques, M., Lopez-Ribot, J.L., and Oliveira, R. (2012). Addition of DNase improves the in vitro activity of antifungal drugs against Candida albicans biofilms. Mycoses *55*, 80–85.

Mashburn-Warren, L., Morrison, D.A., and Federle, M.J. (2010). A novel double-tryptophan peptide pheromone controls competence in Streptococcus spp. via an Rgg regulator. Mol. Microbiol. *78*, 589–606.

Mirau, P.A., and Kearns, D.R. (1983). The effect of intercalating drugs on the kinetics of the B to Z transition of poly(dG-dC). Nucleic Acids Res. *11*, 1931–1941.

Mohanty, T., Fisher, J., Bakochi, A., Neumann, A., Cardoso, J.F.P., Karlsson, C.A.Q., Pavan, C., Lundgaard, I., Nilson, B., Reinstrup, P., et al. (2019). Neutrophil extracellular traps in the central nervous system hinder bacterial clearance during pneumococcal meningitis. Nat. Commun. *10*, 1667.

Moinuddin, A., Arjumand, S., and Ali, A. (1998). SLE autoantibodies binding to native calf thymus DNA brominated in high salt. Lupus *7*, 524–529.

Mokrzan, E.M., Ward, M.O., and Bakaletz, L.O. (2016). Type IV Pilus Expression Is Upregulated in Nontypeable Haemophilus influenzae Biofilms Formed at the Temperature of the Human Nasopharynx. J. Bacteriol. *198*, 2619–2630.

Mokrzan, E.M., Ahearn, C.P., Buzzo, J.R., Novotny, L.A., Zhang, Y., Goodman, S.D., and Bakaletz, L.O. (2020a). Nontypeable Haemophilus influenzae newly released (NRel) from biofilms by antibody-mediated dispersal versus antibody-mediated disruption are phenotypically distinct. Biofilm *2*, 100039.

Mokrzan, E.M., Dairo, K.A., Novotny, L.A., and Bakaletz, L.O. (2020b). Nontypeable Haemophilus influenzae Responds to Virus-Infected Cells with a Significant Increase in Type IV Pilus Expression. MSphere *5*, e00384, 20.

Möller, A., Gabriels, J.E., Lafer, E.M., Nordheim, A., Rich, A., and Stollar, B.D. (1982). Monoclonal antibodies recognize different parts of Z-DNA. J. Biol. Chem. *257*, 12081–12085.

Mulvey, M.A., Schilling, J.D., and Hultgren, S.J. (2001). Establishment of a persistent Escherichia coli reservoir during the acute phase of a bladder infection. Infect. Immun. *69*, 4572–4579.

Newton, K., Wickliffe, K.E., Maltzman, A., Dugger, D.L., Strasser, A., Pham, V.C., Lill, J.R., Roose-Girma, M., Warming, S., Solon, M., et al. (2016). RIPK1 inhibits ZBP1-driven necroptosis during development. Nature *540*, 129–133.

Nickol, J., Behe, M., and Felsenfeld, G. (1982). Effect of the B–Z transition in poly(dG-m5dC). poly(dG-m5dC) on nucleosome formation. Proc. Natl. Acad. Sci. USA *79*, 1771–1775.

Nordheim, A., and Rich, A. (1983). The sequence (dC-dA)n X (dG-dT)n forms left-handed Z-DNA in negatively supercoiled plasmids. Proc. Natl. Acad. Sci. USA *80*, 1821–1825.

Nordheim, A., Lafer, E.M., Peck, L.J., Wang, J.C., Stollar, B.D., and Rich, A. (1982). Negatively supercoiled plasmids contain left-handed Z-DNA segments as detected by specific antibody binding. Cell *31*, 309–318.

Novotny, L.A., Jurcisek, J.A., Pichichero, M.E., and Bakaletz, L.O. (2000). Epitope mapping of the outer membrane protein P5-homologous fimbrin adhesin of nontypeable Haemophilus influenzae. Infect. Immun. *68*, 2119–2128.

Novotny, L.A., Clements, J.D., and Bakaletz, L.O. (2011). Transcutaneous immunization as preventative and therapeutic regimens to protect against experimental otitis media due to nontypeable Haemophilus influenzae. Mucosal Immunol. *4*, 456–467.

Novotny, L.A., Amer, A.O., Brockson, M.E., Goodman, S.D., and Bakaletz, L.O. (2013a). Structural stability of Burkholderia cenocepacia biofilms is reliant

on eDNA structure and presence of a bacterial nucleic acid binding protein. PLoS ONE *8*, e67629.

Novotny, L.A., Clements, J.D., and Bakaletz, L.O. (2013b). Kinetic analysis and evaluation of the mechanisms involved in the resolution of experimental nontypeable Haemophilus influenzae-induced otitis media after transcutaneous immunization. Vaccine *31*, 3417–3426.

Novotny, L.A., Jurcisek, J.A., Goodman, S.D., and Bakaletz, L.O. (2016). Monoclonal antibodies against DNA-binding tips of DNABII proteins disrupt biofilms in vitro and induce bacterial clearance in vivo. EBioMedicine *10*, 33–44.

Oh, D.B., Kim, Y.G., and Rich, A. (2002). Z-DNA-binding proteins can act as potent effectors of gene expression in vivo. Proc. Natl. Acad. Sci. USA *99*, 16666–16671.

Papayannopoulos, V., Staab, D., and Zychlinsky, A. (2011). Neutrophil elastase enhances sputum solubilization in cystic fibrosis patients receiving DNase therapy. PLoS ONE *6*, e28526.

Peck, L.J., Nordheim, A., Rich, A., and Wang, J.C. (1982). Flipping of cloned d(pCpG)n.d(pCpG)n DNA sequences from right- to left-handed helical structure by salt, Co(III), or negative supercoiling. Proc. Natl. Acad. Sci. USA *79*, 4560–4564.

Pohl, F.M., and Jovin, T.M. (1972). Salt-induced co-operative conformational change of a synthetic DNA: equilibrium and kinetic studies with poly (dG-dC). J. Mol. Biol. *67*, 375–396.

Rajendran, A., Endo, M., Hidaka, K., and Sugiyama, H. (2013). Direct and real-time observation of rotary movement of a DNA nanomechanical device. J. Am. Chem. Soc. *135*, 1117–1123.

Ramesh, N., and Brahmachari, S.K. (1989). Structural alteration from non-B to B-form could reflect DNase I hypersensitivity. J. Biomol. Struct. Dyn. *6*, 899–906.

Ray, B.K., Dhar, S., Henry, C., Rich, A., and Ray, A. (2013). Epigenetic regulation by Z-DNA silencer function controls cancer-associated ADAM-12 expression in breast cancer: cross-talk between MeCP2 and NF1 transcription factor family. Cancer Res. *73*, 736–744.

Rice, P.A., Yang, S., Mizuuchi, K., and Nash, H.A. (1996). Crystal structure of an IHF-DNA complex: a protein-induced DNA U-turn. Cell *87*, 1295–1306.

Rich, A., and Zhang, S. (2003). Timeline: Z-DNA: the long road to biological function. Nat. Rev. Genet. *4*, 566–572.

Rmaile, A., Carugo, D., Capretto, L., Zhang, X., Wharton, J.A., Thurner, P.J., Aspiras, M., Ward, M., and Stoodley, P. (2013). Microbial tribology and disruption of dental plaque bacterial biofilms. Wear *306*, 276–284.

Robledo-Avila, F.H., Ruiz-Rosado, J.D., Brockman, K.L., and Partida-Sánchez, S. (2020). The TRPM2 Ion Channel Regulates Inflammatory Functions of Neutrophils During *Listeria monocytogenes* Infection. Front. Immunol. *11*, 97.

Rocco, C.J., Davey, M.E., Bakaletz, L.O., and Goodman, S.D. (2017). Natural antigenic differences in the functionally equivalent extracellular DNABII proteins of bacterial biofilms provide a means for targeted biofilm therapeutics. Mol. Oral Microbiol. *32*, 118–130.

Rocco, C.J., Bakaletz, L.O., and Goodman, S.D. (2018). Targeting the HUβ Protein Prevents Porphyromonas gingivalis from Entering into Preexisting Biofilms. J. Bacteriol. *200*, e00790, 17.

Rosen, D.A., Pinkner, J.S., Jones, J.M., Walker, J.N., Clegg, S., and Hultgren, S.J. (2008). Utilization of an intracellular bacterial community pathway in Klebsiella pneumoniae urinary tract infection and the effects of FimK on type 1 pilus expression. Infect. Immun. *76*, 3337–3345.

Safina, A., Cheney, P., Pal, M., Brodsky, L., Ivanov, A., Kirsanov, K., Lesovaya, E., Naberezhnov, D., Nesher, E., Koman, I., et al. (2017). FACT is a sensor of DNA torsional stress in eukaryotic cells. Nucleic Acids Res. *45*, 1925–1945.

Saunders, S.H., Tse, E.C.M., Yates, M.D., Otero, F.J., Trammell, S.A., Stemp, E.D.A., Barton, J.K., Tender, L.M., and Newman, D.K. (2020). Extracellular DNA Promotes Efficient Extracellular Electron Transfer by Pyocyanin in Pseudomonas aeruginosa Biofilms. Cell *182*, 919–932.e19.

Seviour, T., Winnerdy, F.R., Wong, L.L., Shi, X., Mugunthan, S., Foo, Y.H., Castaing, R., Adav, S.S., Subramoni, S., Kohli, G.S., et al. (2021). The biofilm matrix scaffold of Pseudomonas aeruginosa contains G-quadruplex extracellular DNA structures. NPJ Biofilms Microbiomes *7*, 27.

Shin, S.I., Ham, S., Park, J., Seo, S.H., Lim, C.H., Jeon, H., Huh, J., and Roh, T.Y. (2016). Z-DNA-forming sites identified by ChIP-Seq are associated with actively transcribed regions in the human genome. DNA Res. *23*, 477–486.

Shrestha, P., Emura, T., Koirala, D., Cui, Y., Hidaka, K., Maximuck, W.J., Endo, M., Sugiyama, H., and Mao, H. (2016). Mechanical properties of DNA origami nanoassemblies are determined by Holliday junction mechanophores. Nucleic Acids Res. *44*, 6574–6582.

Sibley, J.T., Lee, J.S., and Decoteau, W.E. (1984). Left-handed "Z" DNA antibodies in rheumatoid arthritis and systemic lupus erythematosus. J. Rheumatol. *11*, 633–637.

Singh, R.K., Liang, D., Gajjalaiahvari, U.R., Kabbaj, M.H., Paik, J., and Gunjan, A. (2010). Excess histone levels mediate cytotoxicity via multiple mechanisms. Cell Cycle *9*, 4236–4244.

Steinberger, R.E., and Holden, P.A. (2005). Extracellular DNA in single- and multiple-species unsaturated biofilms. Appl. Environ. Microbiol. *71*, 5404–5410.

Storisteanu, D.M., Pocock, J.M., Cowburn, A.S., Juss, J.K., Nadesalingam, A., Nizet, V., and Chilvers, E.R. (2017). Evasion of Neutrophil Extracellular Traps by Respiratory Pathogens. Am. J. Respir. Cell Mol. Biol. *56*, 423–431.

Suck, D., and Oefner, C. (1986). Structure of DNase I at 2.0 A resolution suggests a mechanism for binding to and cutting DNA. Nature *321*, 620–625.

Swinger, K.K., and Rice, P.A. (2004). IHF and HU: flexible architects of bent DNA. Curr. Opin. Struct. Biol. *14*, 28–35.

Swinger, K.K., and Rice, P.A. (2007). Structure-based analysis of HU-DNA binding. J. Mol. Biol. *365*, 1005–1016.

Szczesny, B., Marcatti, M., Ahmad, A., Montalbano, M., Brunyánszki, A., Bibli, S.I., Papapetropoulos, A., and Szabo, C. (2018). Mitochondrial DNA damage and subsequent activation of Z-DNA binding protein 1 links oxidative stress to inflammation in epithelial cells. Sci. Rep. *8*, 914.

Temiz, N.A., Donohue, D.E., Bacolla, A., Luke, B.T., and Collins, J.R. (2012). The role of methylation in the intrinsic dynamics of B- and Z-DNA. PLoS ONE *7*, e35558.

Thomas, T.J., and Messner, R.P. (1988). Structural specificity of polyamines in left-handed Z-DNA formation. Immunological and spectroscopic studies. J. Mol. Biol. *201*, 463–467.

Thomas, J.R., Bolla, R.I., Rumbyrt, J.S., and Schlessinger, D. (1985). DNase I-resistant nontranscribed spacer segments of mouse ribosomal DNA contain poly(dG-dT).poly(dA-dC). Proc. Natl. Acad. Sci. USA *82*, 7595–7598.

Thomas, T.J., Gunnia, U.B., and Thomas, T. (1991). Polyamine-induced B-DNA to Z-DNA conformational transition of a plasmid DNA with (dG-dC)n insert. J. Biol. Chem. *266*, 6137–6141.

Timoshenko, S., and Goodier, J. (1970). Theory of Elasticity, Third Edition (McGraw Hill Higher Education).

Tran, T.M., MacIntyre, A., Hawes, M., and Allen, C. (2016). Escaping Underground Nets: Extracellular DNases Degrade Plant Extracellular Traps and Contribute to Virulence of the Plant Pathogenic Bacterium Ralstonia solanacearum. PLoS Pathog. *12*, e1005686.

van der Vorst, E.P.C., Weber, C., and Donners, M.M.P.C. (2018). A Disintegrin and Metalloproteases (ADAMs) in Cardiovascular, Metabolic and Inflammatory Diseases: Aspects for Theranostic Approaches. Thromb. Haemost. *118*, 1167–1175.

Wang, G., Christensen, L.A., and Vasquez, K.M. (2006). Z-DNA-forming sequences generate large-scale deletions in mammalian cells. Proc. Natl. Acad. Sci. USA *103*, 2677–2682.

Whitchurch, C.B., Tolker-Nielsen, T., Ragas, P.C., and Mattick, J.S. (2002). Extracellular DNA required for bacterial biofilm formation. Science *295*, 1487.

Wittig, B., Dorbic, T., and Rich, A. (1991). Transcription is associated with Z-DNA formation in metabolically active permeabilized mammalian cell nuclei. Proc. Natl. Acad. Sci. USA *88*, 2259–2263.

Zacharias, W., Jaworski, A., Larson, J.E., and Wells, R.D. (1988). The B- to Z-DNA equilibrium in vivo is perturbed by biological processes. Proc. Natl. Acad. Sci. USA *85*, 7069–7073.

Zavarykina, T.M., Atkarskaya, M.V., and Zhizhina, G.P. (2019). The Structural and Functional Properties of Z-DNA. Biophysics *64*, 671–682.

Zhang, L., Peeples, M.E., Boucher, R.C., Collins, P.L., and Pickles, R.J. (2002). Respiratory syncytial virus infection of human airway epithelial cells is polarized, specific to ciliated cells, and without obvious cytopathology. J. Virol. *76*, 5654–5666.

Zhang, Y., Cui, Y., An, R., Liang, X., Li, Q., Wang, H., Wang, H., Fan, Y., Dong, P., Li, J., et al. (2019). Topologically Constrained Formation of Stable Z-DNA from Normal Sequence under Physiological Conditions. J. Am. Chem. Soc. *141*, 7758–7764.

Zhou, C., Zhou, F., and Xu, Y. (2009). Comparative analyses of distributions and functions of Z-DNA in Arabidopsis and rice. Genomics *93*, 383–391.

Zhou, H., Sathyamoorthy, B., Stelling, A., Xu, Y., Xue, Y., Pigli, Y.Z., Case, D.A., Rice, P.A., and Al-Hashimi, H.M. (2019). Characterizing Watson-Crick versus Hoogsteen Base Pairing in a DNA-Protein Complex Using Nuclear Magnetic Resonance and Site-Specifically ^{13}C- and ^{15}N-Labeled DNA. Biochemistry *58*, 1963–1974.

Zweig, M., Schork, S., Koerdt, A., Siewering, K., Sternberg, C., Thormann, K., Albers, S.V., Molin, S., and van der Does, C. (2014). Secreted single-stranded DNA is involved in the initial phase of biofilm formation by Neisseria gonorrhoeae. Environ. Microbiol. *16*, 1040–1052.

STAR★METHODS

KEY RESOURCES TABLE

REAGENT or RESOURCE	SOURCE	IDENTIFIER
Antibodies		
Mouse monoclonal [35I9 DNA] to ds DNA	Abcam	Cat # ab27156; RRID:AB_470907
Mouse IgG2a Isotype Control	Invitrogen	Cat # 02-6200; RRID:AB_2532943
Mouse IgG2b Isotype Control	Invitrogen	Cat # 02-6300; RRID:AB_2532949
Rabbit monoclonal α-Z-DNA [Z22]	Absolute Antibodies	Cat # Ab00783-23.0
Murine monoclonal α-Z-DNA [Z22]	Absolute Antibodies	Cat # Ab00783-3.0; RRID:AB_2820286
Rabbit monoclonal isotype control	Abcam	Cat # ab172730; RRID:AB_2687931
Naive sheep serum	Novus	Cat # 5-001-A; RRID:AB_10141430
Sheep polyclonal α-Z-DNA	Abcam	Cat # ab2079; RRID:AB_302819
Rabbit polyclonal human α-neutrophil elastase	Abcam	Cat # ab68672; RRID:AB_1658868
Goat-α-mouse IgG conjugated AlexaFluor405	Invitrogen	Cat # A31553; RRID:AB_221604
Goat-α-mouse IgG conjugated AlexaFluor488	Invitrogen	Cat # A11001; RRID:AB_2534069
Goat-α-rabbit IgG conjugated AlexaFluor488	Invitrogen	Cat # A11008; RRID:AB_143165
Goat-α-rabbit IgG conjugated AlexaFluor647	Invitrogen	Cat # A21245; RRID:AB_2535813
Goat-α-rabbit IgG conjugated AlexaFluor594	Invitrogen	Cat # A11037; RRID:AB_2534095
Goat-α-mouse IgG conjugated AlexaFluor594	Invitrogen	Cat # A11032; RRID:AB_2534091
Wheat germ agglutinin, Alexa Fluor 350 Conjugate	Invitrogen	Cat # W11263
Mouse IgG1 Isotype Control	Thermo Fisher Scientific	Cat # 02-6100; RRID:AB_2532935
goat α-mouse IgG-conjugated to HRP	Invitrogen	Cat # 31430; RRID:AB_10974121
Rabbit Anti-Sheep IgG H&L (HRP)	Abcam	Cat # ab6747; RRID:AB_955453
Protein A-HRP	Invitrogen	Cat # 101023
Normal Goat serum	Life Technologies	Cat # 50062Z
Bacterial and virus strains		
S. mutans strain UA159	Mashburn-Warren et al., 2010	N/A
NTHI Strain 86-028NP	Harrison et al., 2005	N/A
UPEC strain UTI89	Mulvey et al., 2001	UTI89
P. aeruginosa strain ATCC 27853	ATCC	27853
Clinical isolate of *K. pneumoniae*	Rosen et al., 2008	N/A
Biological samples		
Human sputum from individuals with Cystic Fibrosis	This study	Cure CF Columbus Translational Core
Chinchilla otitis media samples	This study	Nationwide Children's Hospital in accordance with 01304AR
Chemicals, peptides, and recombinant proteins		
Cerium Chloride	Alpha Aesar	CAS 7790 −86-5
Chloroquine	Sigma	C6628-100G25G
Pulmozyme dornase alfa	Genentech	NDC Code 50242-100-40

(*Continued on next page*)

Continued

REAGENT or RESOURCE	SOURCE	IDENTIFIER
Bromine water	RICCA	Cat# 1195-16
FM4-64	Invitrogen	T3166
LIVE/DEAD	Invitrogen	L7007
Recombinant HU_{NTHI}	Novotny et al., 2016	N/A
Recombinant CbpA	Devaraj et al., 2018	N/A
Recombinant RusA	Devaraj et al., 2019	N/A
3,3′,5,5′-tetramethylbenzidine	MP Biomedicals	0215234650
ELISA Stop solution (H_2S0_4)	Bethyl Laboratories	E115
1-Step TMB-Blotting Substrate Solution	Thermo Fisher Scientific	34018
Image-iT FX Signal Enhancer	Invitrogen	I36933
ProLong Diamond	Invitrogen	P36961
Super Block	ScyTec Laboratories	AAA999
Invitrogen ProLong Gold Antifade Mountant	Invitrogen	P36930
DAPI	Thermo Scientific	62248
NucBlue Live	Invitrogen	R37605
Sytox Green Nucleic Acid Stain	Invitrogen	S7020
Bovine Serum Albumin	Fisher Scientific	BP9703100
Critical Commercial Assays	N/A	N/A
EasySep Human neutrophil isolation kit	StemCell Technologies	17957
MasterPure Gram Positive DNA Purification Kit	Epicenter	MGP04100
Deposited data		
https://dx.doi.org/10.17632/fpwbypb4kd.1	Mendeley DATA	https://data.mendeley.com/
Experimental models: Cell lines		
Primary human airway epithelial cells (HAEs)	This study	C3 Epithelial Cell Core at Nationwide Children's Hospital
Human-derived Neutrophils isolated from healthy adult control subjects	This study	Blood donation at Nationwide Children's Hospital (IRB #00002860)
Experimental models: Organisms/strains		
Adult (501-859 g) mixed sex chinchillas (*Chinchilla lanigera*)	Rauscher's Chichilla Ranch, LLC. La Rue, Ohio	USDA license #31A0040
Oligonucleotides		
PolydGdC	InvivoGen	tlrl-pgcn
Genomic DNA isolated from NTHI 86-028NP	This study	N/A
Software and algorithms		
BMG Labtech Fluostar Omega plate reader with Omega software	BMG Labtech	N/A
Zeiss LSM 800 with ZEN 2.6 Software	Zeiss	N/A
Protein Simple FluoroChem M Imager and Digital Darkroom software v 4.1.4.	Protein Simple	N/A
TA Instruments Discovery Hybrid Rheometer-2 (HR-2) with Peltier plate	TA Instruments	HR2
RIOSv4	TA Instruments	N/A
Axiovision4	Zeiss	N/A
ZEN Black edition	Zeiss	N/A
ImageJ	NIH	https://imagej.nih.gov/ij/
Metamorphose2	GPLv3	2.0.8.2

(*Continued on next page*)

Continued

REAGENT or RESOURCE	SOURCE	IDENTIFIER
Comstat2 plugin	Technical University of Denmark	https://www.comstat.dk
GraphPad Prism 8 and 9	GraphPad Software 8.1 and 9.1	https://www.graphpad.com:443/
MARS	BMG Labtech	https://www.bmglabtech.com/microplate-reader-software/
Biorender	Biorender.com	Biorender2021
Paint3D	Microsoft Corporation	5.1902.13017.0
Other		
FluoroDish	WPI	FD35-100
LabTek Chambered coverglass	Thermo Scientific	155411
Costar Transwell Permeable Supports	Corning	3470
Nunc 96 Well UV transparent plate	ThermoFisher Scientific	8404
Nunc MaxiSorp C-bottom 96 well plate	ThermoFisher Scientific	44-2404-21
Fisherbrand Superfrost Plus Microscope Slides	Fisher Scientific	22-037-246

RESOURCE AVAILABILITY

Lead contact

Further information and requests for resources and reagents should be directed to and will be fulfilled by the Lead Contact, Steven D. Goodman (Steven.Goodman@NationwideChildrens.org).

Materials availability

All unique/stable reagents generated in this study are available from the Lead Contact with a completed Materials Transfer Agreement.

Data and code availability

The published article includes all datasets generated or analyzed during this study except for additional original replicate data (Figures 1, 5, S2, S3, and S7) which is deposited within Mendeley Data: https://doi.org/10.17632/fpwbypb4kd.1.

EXPERIMENTAL MODEL AND SUBJECT DETAILS

Bacterial strains

NTHI strain 86-028NP (Harrison et al., 2005), NTHI 86-028NP/pMDC-P1(Mokrzan et al., 2016), *S. mutans* strain UA159 (Mashburn-Warren et al., 2010), UPEC strain UTI89 (Mulvey et al., 2001), *P. aeruginosa* strain ATCC 27853, and a clinical isolate of *K. pneumoniae* (Rosen et al., 2008) were used.

Human-derived samples

Well-differentiated primary human airway epithelial cells (HAEs) from healthy donors were obtained from the C3 Epithelial Cell Core at Nationwide Children's Hospital. Human sputum from individuals with a diagnosis of cystic fibrosis were obtained from the Cure CF Columbus Translational Core CF sputum samples through IRB11-00790. Human neutrophils were isolated from blood donated from healthy adult control subjects that span the demographic spectrum of central Ohio to the Abigail Wexner Research Institute Blood Donor service after obtaining informed consent and under approved IRB protocol (#00002860) at Nationwide Children's Hospital.

Chinchilla model

Adult (501-859 g) outbred, mixed sex chinchillas (*Chinchilla* langigera) are procured from a single vendor, Raushcher's Chinchilla Ranch, LLC., located in La Rue, Ohio (USDA license #31A0040). To induce experimental otitis media (OM), chinchillas are injected transbullarly with a small inoculum of nontypeable *Haemophilus influenzae* (NTHI; strain #86-028NP) to deliver ~1000 CFU. In this model, NTHI will form a mucosal biofilm that fill > 50% of the middle ear within 4 days of challenge (Novotny et al., 2011). On either day 11 or 14 after challenge, animals were sacrificed per approved IACUC protocol, and mucosal biofilms were collected, frozen in OCT at the time of collection and processed for imaging as we have described earlier (Goodman et al., 2011). Chinchilla Otitis media samples were collected in accordance with the NIH Guide for the Care and Use of Laboratory Animals and under protocol 01304AR at Nationwide Children's Hospital.

METHOD DETAILS

Bacterial growth

NTHI was grown in Brain Heart Infusion (sBHI) broth supplemented with hemin (2 μg/ml) and β-NAD (2 μg/ml). UPEC and *K. pneumoniae* were grown in Luria Broth (LB), *P. aeruginosa* was grown in Tryptic Soy Broth (TSB), and *S. mutans* was grown in Todd Hewett Broth (THB). Cultures were grown at 37°C in a 5% CO_2 humidified incubator.

In vitro biofilms

Biofilms were allowed to form in a LabTek n 8-well glass chambered slide (Fisher Scientific 155411) and maintained for 24-40h with replenishment of the respective media at 16 and 24h post biofilm initiation. *S. mutans* biofilms were maintained for 40h, with replenishment of media at 24h. NTHI was grown as indicated above then diluted to 2.5 × 105 CFU/ml in 200 μL sBHI. UPEC and *K. pneumoniae* were cultured on LB agar overnight at 37°C in 5% CO_2 humidified atmosphere then suspended in LB broth to an OD_{490} of 0.65, diluted (1:12 in LB), and incubated statically for 2.5h. The cultures were then diluted to 2.5 × 105 CFU/ml in 200 μL LB and inoculated into an 8-well glass chamber slide. *P. aeruginosa* biofilms were grown as above but were not incubated statically for the additional 2.5h. After 40h, the pellicle at the air-liquid interface was collected onto a glass slide. For *S. mutans*, an overnight culture was diluted 1:25 in THB broth then incubated at 37°C in 5% CO2 to an OD_{490} of 0.65. The culture was then diluted to OD_{490} 0.05 and seeded into an 8-well glass chamber slide.

Antibodies

The following commercial antibodies were used: murine monoclonal antibody against ds-DNA [3519] (B-DNA) (Abcam, ab27156), murine monoclonal isotype IgG2a (Invitrogen, 02-6200) and 2b (Invitrogen, 02-6300)), rabbit monoclonal antibody against α-Z-DNA[Z22] (Absolute Antibodies, Ab00783-23.0), murine monoclonal antibody against Z-DNA [Z22] (Absolute Antibodies, Ab00783-3.0), rabbit monoclonal IgG isotype control (Abcam, Ab172730), naive sheep serum (Novus, 5-001-A), sheep polyclonal antibody against Z-DNA (Abcam, Ab2079), rabbit polyclonal α-neutrophil elastase (Abcam, Ab68672). IgG was purified from unimmunized rabbit whole serum as previously described (Devaraj et al., 2018).

Nuclease resistance of biofilms

NTHI 86-028NP and UPEC strains were grown as described. Biofilm growth was initiated in the presence or absence of Pulmozyme® (Genentech, dornase alfa, NDC Code 50242-100-40) [50 or 125 μg/ml] for 16h for prevention assays or added at 24h for disruption assays. Biofilms were then washed twice with 0.9% (w/v) saline, stained with LIVE/DEAD® (Invitrogen, L7007) per manufacturer's instructions, fixed, visualized by confocal laser scanning microscope (CLSM) [Zeiss LSM 800 with Zen 2.6 Software, and images analyzed with COMSTAT software (Heydorn et al., 2000).

Antibody specificity of B- and Z-DNA antibodies

Induction of Z-form DNA from genomic DNA (gDNA) [purified from NTHI using the MasterPure Gram Positive DNA Purification Kit (Epicenter, MGP04100) and poly(dGdC) (InvivoGen, tlrl-pgcn)] was as previously described by bromination of DNA substrates in the presence of 4M NaCl (Edgington and Stollar, 1992) with a few modifications as follows. Poly(dGdC) DNA or gDNA substrates (200 μg) were incubated overnight in 10.5ml 20mM Na citrate buffer with 4M NaCl supplemented with 500μl bromine water (RICCA, 1195-16) at room temperature, followed by buffer exchange with QIAamp Midi spin column (QIAGEN) and quantification with Biotek Epoch Take3 plate reader. Z-DNA formation was determined by the absorbance ratio of 260 to 295nm as described previously (Chaires, 1983; Pohl and Jovin, 1972) for non-brominated or brominated poly(dGdC) (1 μg) substrates in a 100 μL volume of a10mM Na-Cacodylate, 10mM NaCl, and 2mM EDTA buffer of within a Nunc 96 well UV transparent plate (ThermoFisher Scientific, 8404). Absorbance values were obtained by a Biotek Synergy H1 spectrophotometer at 260 and 295nm wavelengths. Buffer without DNA substrates served as blanks. Specificity of monoclonal antibodies was confirmed by ELISA using a Nunc MaxiSorp C-bottom 96 well plate (ThermoFisher Scientific, 44-2404-21) coated with 1 μg of poly dGdC (B-DNA) or brominated poly dGdC (Z-DNA^{102}), followed by blocking with 0.5% (w/v) BSA in PBS for 1h at 37°C. Wells were then probed with murine IgG1(ThermoFisher Scientific, 02-6100) [neg. control], murine monoclonal antibody against either B-DNA[3519] (Abcam, ab27156) or Z-DNA[Z22] (Absolute Antibodies, Ab00783-3.0) for 1h at 37°C, and detected with goat α-mouse IgG-conjugated to HRP (Invitrogen, 31430) at 1:1000. TMB (3,3′,5,5′-tetramethylbenzidine) (MP Biomedicals, Inc., 0215234650) was the colorimetric substrate used for HRP detection. The stop solution was 2M H_2SO_4 (Bethyl Laboratories, E115). Absorbance values at 450nm were obtained on a BMG Labtech Fluostar Omega plate reader. An image of a representative microtiter plate was captured on a Protein Simple FluorChemM instrument.

Pulmozyme protection assay

Poly-dGdC (2 ug) and br-poly-dGdC (2 ug), prepared as described above were incubated in a buffer containing 10 mM cacodylate pH 7.0, 10 mM NaCl and 100 μM $CaCl_2$, with and without 0.5 units Pulmozyme® (Genentech, dornase alfa, NDC Code 50242-100-40) for 10 minutes at 37°C. EDTA at a final concentration of 5 mM was then added to each tube to quench the reactions. A 20μl aliquot of each was electrophoresed on a 1% agarose gel containing ethidium bromide at120V for 30 minutes. The resulting gel was imaged on a BioRad Gel Doc instrument, using ImageLab software.

Verification of antibody cross-reactivity by western blot

Bacterial cell lysates were prepared by collection of a NTHI biofilms formed for 40h in chambered coverglass slides as described (Devaraj et al., 2018). Lysates were heated to 100°C for 5 min in 4X Laemmli Sample buffer (BioRad) and 20ug protein applied per well of 12% sodium dodecyl sulfate–polyacrylamide gel. Proteins were electrophoretically separated in Tris-glycine-SDS buffer (BioRad), transferred to PVDF membrane (BioRad) and blocked with 2% bovine serum albumin (Millipore-Sigma) in Tris-buffered saline. Membranes were probed with murine monoclonal antibody to B-DNA (as determined in ''antibody specificity of B- and Z-DNA antibodies''), murine monoclonal antibody to Z-DNA or murine IgG2a isotype antibody control. Additionally, reactivity of IgG isolated from sheep anti-Z DNA or unimmunized sheep serum was assessed. As a positive antibody control, chinchilla antiserum raised against NTHI 86-028NP whole outer membrane protein preparation was incorporated (Novotny et al., 2000). Murine antibodies were revealed with goat anti-mouse IgG-HRP (Invitrogen, 31430), sheep antibodies were detected with rabbit anti-sheep IgG-HRP (Abcam, Ab6747) and chinchilla antibodies shown with Protein A-HRP (Invitrogen, 101023) and developed with Pierce 1-Step Ultra TMB Blotting Solution (ThermoFisher Scientific, 34018. Images were captured on a Protein Simple FluorChemM instrument.

B-DNA and Z-DNA increases during biofilm maturation

Biofilms of strains NTHI 86-029 NP, UPEC UTI89, and *Klebsiella pneumoniae* were allowed to form in an 8-well glass chamber slide as described above for 24, 40, 90h, and 1 week. At each indicated time-point, biofilms were washed once with phosphate buffered saline (PBS) and probed with either murine monoclonal antibody against B-DNA[3519] (Abcam, ab27156) [5 μg] or murine monoclonal antibody against Z-DNA[Z22] (Absolute Antibodies, Ab00783-3.0) [5 μg] and their respective murine isotype IgG2a (Invitrogen, 02-6200) or IgG2b (Invitrogen, 02-6300) [5 μg] controls in 1ml of a diluent that contained 5% (bovine serum albumin) [Fisher Scientific, BP9703100] BSA (w/v) in PBS for 1h at room temperature. The biofilms were then washed once with PBS and incubated in PBS that contained 5% (w/v) BSA with 1:200 dilution of the respective goat-α mouse IgG conjugated Alexa Fluor® 488 (Abcam, A11001) for 1hr at room temperature, and stained with 1:400 dilution of FM4-64 (Invitrogen, T3166). The biofilms were then washed once with PBS and imaged using a 63x oil objective on a Zeiss LSM 800 confocal microscope (Carl Zeiss Inc.).

Visualization of B-DNA and Z-DNA in biofilms formed *in vitro*

To probe for B-DNA and Z-DNA, biofilms were allowed to form as described above, then washed once with PBS and incubated with rabbit monoclonal antibody raised against Z-DNA[Z22] (Absolute Antibodies, Ab00783-23.0) (5 μg), IgG purified from unimmunized rabbit serum (5 μg), with murine monoclonal antibody raised against B-DNA[3519] (Abcam, ab27156) (5 μg), or murine isotype IgG2a (Invitrogen, 02-6200) (5 μg) in 1 mL of PBS that contained 5% (w/v) BSA for 2 hours at room temperature. Biofilms were washed with PBS and incubated with either a 1:200 dilution of goat α-rabbit IgG conjugated to Alexa Fluor® 488 (Invitrogen, A11008) or goat α-mouse IgG conjugated to Alexa Fluor® 405 (Invitrogen, A31553), and counterstained with 5 μg FM4-64 (Invitrogen, T3166) /ml PBS that contained 5% BSA. Biofilms were then washed once with PBS and imaged using a 63x oil objective on a Zeiss LSM 800 microscope.

Visualization of B-DNA and Z-DNA in biofilms formed on HAEs

Well-differentiated primary human airway epithelial cells (HAEs) from one healthy donor were obtained from the C3 Epithelial Cell Core at Nationwide Children's Hospital. Cells were added to 6.5mm^2 diameter Costar Transwell permeable inserts (Corning Inc., 3470) with a pore size of 0.4 μm then incubated as described to permit polarization (Mokrzan et al., 2016; Zhang et al., 2002) and differentiation. Prior to inoculation with NTHI, the apical surface of the polarized HAEs was first gently washed with PBS to remove excess accumulated mucus. NTHI 86-028NP/pMDC-P1, a reporter construct wherein the promoter for NTHI *ompP5* drives expression of green fluorescent protein (Mokrzan et al., 2016) was inoculated on to HAE cultures at a MOI of 100 bacteria per epithelial cell, and incubated for 16 h. Non-adherent NTHI were removed by aspiration and the apical surface of the HAE cultures blocked with 10% normal goat serum (Bethyl Laboratories, Inc., IHC-GS50)- 0.05M Tris-0.15M NaCl, pH 7.4 buffer. Cultures were incubated with antibody cocktails that contained murine monoclonal antibody to B-form DNA [3519] (Abcam, ab27156) and rabbit monoclonal antibody to Z-form DNA[Z22] (Absolute Antibodies, Ab00783-23.0) (5 μg each antibody/ml buffer). Negative antibody controls consisted of murine IgG1 isotype antibody (ThermoFisher Scientific, 02-6100) and IgG enriched from unimmunized rabbit serum (5 μg each antibody/ml buffer). Labeling was revealed with goat anti-rabbit IgG conjugated to Alexa Fluor® 647 (Invitrogen, A21245) and goat anti-mouse IgG conjugated to Alexa Fluor® 594 (Invitrogen, A11032) [5 μg each antibody /ml]. One set of HAE cultures was not inoculated with NTHI; however, it was probed with antibodies to B-form and Z-form DNA to validate that any DNA-specific signal observed was due to DNA release from NTHI and not from epithelial cells. Transwell membranes were excised, mounted on to SuperFrost Plus slides (Fisher Scientific, 22-037-246) with ProLong Diamond (Invitrogen, P36961) and coverslipped prior to visualization on a Zeiss LSM800 confocal scanning laser microscope.

Visualization of B-DNA and Z-DNA within clinical specimens

To examine for the presence of B- or Z-forms of DNA within biofilms formed during disease, archived specimens frozen in OCT at the time of collection were examined: (1) a 14-day old NTHI biofilm formed in the middle ear of a chinchilla during experimental otitis

media and (2) sputum from an individual with CF wherein the specimen was culture positive for MSSA and *Burkholderia cenocepacia* complex. Ten μm serial sections were cut and processed via standard protocol (Jurcisek and Bakaletz, 2007). Briefly, slides were air-dried, fixed in cold acetone, then equilibrated in 0.05M Tris-HCl, 0.15M NaCl-, 0.05% Tween 20 buffer, pH 7.4. Sections were blocked with image-iT FX signal enhancer (Invitrogen, I36933)) followed by Super Block (ScyTec Laboratories, Inc., AAA999). Specimens were incubated with primary antibody cocktail comprised of murine monoclonal antibody against B-DNA [3519] (Abcam, ab27156) (5.0 μg/ml), rabbit monoclonal antibody against Z-DNA (5.0 μg/ml) diluted in 5% (w/v) BSA in PBS. IgG purified from serum from unimmunized rabbit or murine IgG1antibody (ThermoFisher Scientific, 02-6100) served as the respective negative antibody controls for non-specific binding. Labeling was revealed with goat anti-rabbit IgG conjugated to Alexa Fluor® 647 (Invitrogen, A21245), goat anti-mouse IgG conjugated to Alexa Fluor® 488 (Invitrogen, A11001) [each used at 5 μg/ml] in PBS. Prolong Gold (Invitrogen, P36930) or Prolong Gold with NucBlue Live (Invitrogen, R37605) was applied prior to placement of a coverslip. Sections were viewed using a Zeiss LSM 800 confocal microscope and images rendered with Zeiss Zen 2.6 software.

Quantification of Z-DNA and B-DNA within nuclease-treated biofilms

NTHI 86-029 NP, UPEC, and *K. pneumoniae*, were allowed to form biofilms, then maintained for 40 hours as described above in "*in vitro* biofilms." At 24 hours, biofilms were incubated in the presence or absence of Pulmozyme® (Genentech, dornase alfa) [40U/ml] for 16h at 37°C. Alternatively, to determine whether B-DNA was a reservoir for Z-DNA development, Pulmozyme® (Genentech, dornase alfa, NDC Code 50242-100-40) was added at initiation followed by subsequent additions at 16 and 24h for a total of 40h. The biofilms were then washed with PBS and incubated with 200 μl of PBS that contained 5% (w/v) BSA and either murine monoclonal antibody raised against B-DNA [3519] (Abcam, ab27156) [5 μg/ml] or rabbit monoclonal antibody raised against Z-DNA [Z22] (Absolute Antibodies, Ab00783-23.0) [5 μg/ml] or the respective naive murine IgG isotype 2aIgG2a (Invitrogen, 02-6200) (5μg/ml) or IgG purified from unimmunized rabbit [5μg/ml] controls for 1h at room temperature. The biofilms were then washed once with PBS and incubated with the respective goat-α mouse IgG conjugated Alexa Fluor® 405 (Invitrogen, A31553) and goat-α rabbit IgG conjugated Alexa Fluor® 488 (Invitrogen, A11008) in PBS that contained 5% (w/v) BSA for 1h at room temperature, and counterstained with 5 μg of FM4-64(Invitrogen, T3166) /ml in PBS. The biofilms were then washed with PBS and imaged using a 63x oil objective on a Zeiss LSM 800 confocal microscope (Carl Zeiss Inc.). The fluorescence intensity of B-DNA (Alexa Fluor® 405 signal) and Z-DNA (Alexa Fluor® 488 signal) were normalized to the fluorescence intensity of FM4-64. Changes in fluorescence intensity was determined by ImageJ software by determining the mean intensity of Z stacks. NTHI 86-028NP was incubated as described previously. Biofilm growth was initiated in the presence or absence of Pulmozyme® (Genentech, dornase alfa, NDC Code 50242-100-40) [100 μg/ml], followed by subsequent additions at 16 and 24h for a total of 40h. The biofilms were washed, incubated with the appropriate monoclonal antibodies, and visualized as described in "Quantification of Z-DNA and B-DNA within nuclease treated biofilms."

Stimulation of biofilm formation by anti-Z-DNA

NTHI and UPEC biofilms were initiated in the presence of 0, 1, or 5 μg/ml polyclonal α-Z DNA antibody IgG (Abcam, ab2079) or unimmunized sheep IgG (Novus, 5-001-A) and grown for 16h. Additionally, UPEC biofilms were initiated in the presence of 0 or 5 μg/ml murine monoclonal α-Z-DNA[Z22] (Absolute Antibodies, Ab00783-3.0) or murine isotype 2b (Invitrogen, 02-6300). Biofilms were then analyzed by LIVE/DEAD® (Invitrogen, L7007) as described above in "nuclease resistance in biofilms."

Confirmation of B/Z-DNA conversion by OD 260/295

Genomic DNA (400ng) was incubated in a reaction buffer as described previously "Antibody specificity of B- and Z-DNA antibodies" and supplemented with 0, 0.25, 0.5, and 1mM $CeCl_3$ for 2h at 37°C. Poly(dGdC) (1 μg) was incubated with either NaCl (3.6M), chloroquine (100 μM), or a combination of both for 2h at 37°C. The absorbance values were obtained as described above in "Antibody specificity of B and Z-DNA antibodies." Reaction buffers that contained chloroquine or NaCl (absent DNA) served as blanks. The values were plotted as the ratio of A260/295.

Growth curves of planktonic NTHI

Planktonic growth curves of NTHI were initiated at OD_{490} of 0.02 in sBHI supplemented with 0, 250, 500, or 1000 μM $CeCl_3$ or with 0, 10, 50, 100, or 200 μM chloroquine in a 96-well plate and grown for 16h at 37°C using a Biotek Synergy H1 multi-mode plate reader.

Modulation of B/Z eDNA of bacterial biofilms

Cultures of NTHI were incubated as described above. At 24h, $CeCl_3$ (Alpha Aesar, CAS 7790-86-5), a compound known to induce Z-DNA (Bhanjadeo et al., 2017), was added to a final concentration of 0.25, 0.5, or 1mM in sBHI to convert B- to Z-DNA. Chloroquine (Sigma, C6628-100G), a known inhibitor of Z-DNA formation (Kwakye-Berko and Meshnick, 1990) was added to a final concentration of 1μM or 5 μM in sBHI to convert Z-DNA to B-DNA. The effect of DNABII proteins on Z-DNA within the biofilm EPS was analyzed by the exogenous addition of HU_{NTHI} (Novotny et al., 2016) [2 μg/ml] at initiation and throughout biofilm development as previously described (Devaraj et al., 2018). Biofilms were probed for Z-DNA with IgG purified from unimmunized rabbit serum (5 μg/ml) or rabbit α-Z-DNA [Z22] (Absolute Antibodies, Ab00783-23.0) [5 μg/ml] in 5% (w/v) BSA in PBS, then goat α-rabbit conjugated with Alexa

Fluor® 488 (Invitrogen, A11008), and stained with FM4-64 (Invitrogen, T3166) before being analyzed by immunofluorescence microscopy with calculation of partition coefficients determined as described previously (Devaraj et al., 2015).

Axial mechanical indentation of NTHI biofilms

NTHI biofilms were grown in 35 mm FluoroDishes (World Precision Instruments, FD35-100) for 40 h at 37°C with 5% CO_2 as described above. After 24h, biofilms were treated with $CeCl_3$ (500μM) for 16h, then incubated with media or Pulmozyme® (50μg/ml) for 1h at 37°C with 5% CO_2. Media only treatment was used as a control. To test the effect of chloroquine, NTHI biofilms were grown for 40 h and treated with cholorquine (5μM) for 1 h at 37°C with 5% CO_2. NTHI biofilms were initiated in the presence of RusA (10μg/ml) or HU_{NTHI} (2μg/ml) and supplemented at 16 and 24h for a total of 40h. Additionally, HU_{NTHI} was added as throughout biofilm development as described in "Modulation of B/Z eDNA of bacterial biofilms" for 40h then were treated with Pulmozyme® (50μg/ml) or RusA (10μg/ml) + Pulmozyme® (50μg/ml) for 1h. Additionally, NTHI biofilms were grown for 24h, incubated with $CeCl_3$ (500μM) for 16h, then treated with RusA (10μg/ml) for 1h at 37°C with 5% CO_2. Biofilms were then washed twice with PBS and maintained in 600 μl mL PBS until rheological analysis.

Axial mechanical indention was performed on treated NTHI biofilms as previously described (Devaraj et al., 2019). Briefly, the FluoroDish containing treated or control biofilms was transferred to the Peltier plate of a Discovery Hybrid Rheometer-2 (DHR-2; TA instruments) fitted with an 8 mm sand-blasted Smart Swap parallel plate geometry. The geometry was lowered onto the submerged biofilm at an approach rate of 1 μm/s. Three biological replicates were performed, each with duplicate replicates. Two to three measurements were taken for each biofilm. TRIOS v5 (TA instruments) software was used.

For data interpretation, force-displacement curves were converted to stress-strain curves as previously described (Gloag et al., 2018). The Young's modulus (E) was determined using the previously described force-displacement relationship, according to Equation S1 (Timoshenko and Goodier, 1970),

$$E = \frac{slope \cdot (1 - v^2)}{2r} \qquad \text{Equation S1}$$

where r is the radius of the geometry (0.004 m), and v is the assumed Poisson's ratio for a biofilm (v = 0.5) (Rmaile et al., 2013). The slope is of the force-displacement curve (N/m), taken at the lower "linear" portion corresponding to 0%–40% strain.

The susceptibility of biofilms to DNase after chloroquine

NTHI biofilms were established as described above. At 40h, chloroquine (Sigma, C6628-100G) [5 μM], Pulmozyme®(Genentech, dornase alfa, NDC Code 50242-100-40) [50 μg/ml] or a combination of both in sBHI were added to mature biofilms and incubated for 1h at 37°C. Biofilms were then washed twice with 0.9% (w/v) saline, stained with LIVE/DEAD® (Invitrogen, L7007) per manufacturer's instructions, fixed, visualized by confocal laser scanning microscope (CLSM), and images analyzed by COMSTAT (Heydorn et al., 2000).

The susceptibility of clinical specimens to DNase and chloroquine

Fresh human sputum from 4 individuals with a diagnosis of cystic fibrosis were obtained from the Cure CF Columbus Translational Core, divided into approximately equal volumes and placed into wells of a 24-well plate as described (Gustave et al., 2013). The remainder of each specimen was snap-frozen in OCT and processed for immunofluorescent detection of B-DNA and Z-DNA as described above. To evaluate the susceptibility of each fresh sputum specimen to disruption, the following treatments were applied: 10μM chloroquine, 100μM chloroquine, 10U Pulmozyme® (Genentech, dornase alfa, NDC Code 50242-100-40), 30U Pulmozyme®, 10μM chloroquine+10U Pulmozyme®, 100μM chloroquine+10U Pulmozyme®, 10μM chloroquine+30U Pulmozyme® or 100μM chloroquine+30U Pulmozyme® or diluent (DPBS) only. Sputa were incubated static for 1h at 37°C and changes in the optical density in the solution that surrounded the sputum solids were determined at 600nm in a 6x6 matrix 14mm in diameter with a BMG Labtech Fluorostar Omega plate reader. Images of sputum specimens were captured using a Zeiss SV6 microscope and Zeiss Zen software. As part of routine clinical analysis, an aliquot of each sputum specimen was also submitted for speciation to the Laboratory Services at Nationwide Children's Hospital.

Prevention of Z-DNA formation by a HJ resolvase

NTHI 86-028NP was incubated as described previously. RusA was purified as described (Devaraj et al., 2019). Biofilm growth was initiated in the presence or absence of RusA (10μg/ml) for 16h. The biofilms were washed, incubated with murine monoclonal antibody raised against B-DNA [3519] (Abcam, ab27156) [5 μg/ml] and rabbit monoclonal antibody raised against Z-DNA [Z22] (Absolute Antibodies, Ab00783-23.0) [5 μg/ml] or the respective murine IgG isotype IgG2a (Invitrogen, 02-6200) [5μg/ml] or IgG purified from unimmunized rabbit [5μg/ml] controls for 1h at room temperature. The biofilms were then washed once with PBS and incubated with the respective goat-α mouse IgG conjugated Alexa Fluor® 405 (Invitrogen, A31553) and goat-α rabbit IgG conjugated Alexa Fluor® 488 (Invitrogen, A11008) in PBS that contained 5% (w/v) BSA for 1h at room temperature, and counterstained with 5 μg of FM4-64 (Invitrogen, T3166) /ml in PBS. The biofilms were then washed with PBS and imaged using a 63x oil objective on a Zeiss LSM 800 confocal microscope (Carl Zeiss Inc.). The fluorescence intensity of B-DNA (Alexa Fluor® 405 signal) and Z-DNA (Alexa Fluor® 488 signal) were

normalized to the fluorescence intensity of FM4-64. Changes in fluorescence intensity was determined by ImageJ software by determining the mean intensity of Z stacks.

DNABII proteins drive B-DNA dominant NETs to Z-DNA during PMA-induced NETosis

Human neutrophils were isolated from blood using the EasySep™ Human neutrophil isolation kit (StemCell Technologies, Inc. Inc., 17957). Neutrophils ($1x10^5$) were incubated and allowed to attach to 8-well glass chamberslides followed by induction of NETs with 200nM PMA (phorbol-12-myristate-13-acetate) for 3.5h in the presence or absence of 500nM HU_{NTHI} (Novotny et al., 2016) or CbpA [purified as described (Devaraj et al., 2018)] and served as a negative control. NETs were formalin fixed, blocked with 10% normal goat serum (Life Technologies, 50062Z), and incubated with rabbit monoclonal antibody raised against Z-DNA [Z22] (Absolute Antibodies, Ab00783-23.0) (5 μg), from rabbit isotype control (Abcam, ab172730) [5 μg], with murine monoclonal antibody raised against B-DNA [3519] (Abcam, ab27156) [5 μg], or murine isotype IgG2a (Invitrogen, 02-6200) [5 μg] in 1 mL of PBS for 16h hours at 4°C. NETs were washed with PBS and incubated for 1h with 1:200 dilution of goat α-rabbit IgG conjugated to Alexa Fluor® 594 (Invitrogen, A11037) or goat α-mouse IgG conjugated to Alexa Fluor® 488 (Invitrogen, A11001) and 1:1000 dilution wheat germ agglutinin conjugated to Alexa Fluor® 350 (Invitrogen, W11263) [PMN membrane stain]. As a control, common NETs markers were used to verify proper activation. NETs were incubated similarly with 1:100 rabbit polyclonal antibody raised against human neutrophil elastase (Abcam, ab68672) to label elastase which is indicative of active NETs DNA structure. 1:5000 SYTOX™ green nucleic acid stain (Invitrogen, S7020), and 1:1000 wheat germ agglutinin conjugated to Alexa Fluor® 350 (Invitrogen, W11263) to counterstain the plasma membrane of the neutrophils. NETs were imaged with a Zeiss LSM 800 confocal microscope (Carl Zeiss Inc.) and rendered with Zeiss Zen 2.6 software.

NET inactivation of bacterial killing

NTHI biofilms were allowed to establish for 16h as described above. Briefly, $2.5x10^5$ bacteria were incubated for 16h in a 24 well glass-plates prior to the addition of neutrophils. Peripheral blood neutrophils were purified from healthy donors by magnetic negative selection (StemCell Technologies, Inc. Inc., 17957) and adjusted to be able to deliver $1x10^6$ PMNs/well. Prior to the addition of PMNs, the young biofilms were washed carefully with PBS to remove non-adherent bacteria, followed by the addition of 300 μl of RPMI supplemented with 10% FBS. Neutrophils were then added to the wells and treated with either: 1μM HU_{NTHI}, 1 μM CbpA, or 10 units Pulmozyme® (Genentech, dornase alfa, NDC Code 50242-100-40)/ml for 4h. After incubation, during which time biofilm remodeling occurs, 0.1% Triton X-100 was added to the cultures to release any intracellular bacteria from the PMNs after which all bacteria were recovered by homogenized via pipetting, followed by serial dilutions and plating (Robledo-Avila et al., 2020). The percentage of reduction of the number of NTHI (total CFU) and % relative killing was calculated as indicated in the following formulas: [(CFU of each sample) ÷ (average CFU of NTHI only controls) x 100 = % viable]: [% Killing = 100% - (% viable)]. The relative % killing was normalized so that the NTHI only control represented 0% killing as follows: [100% (e.g., average of NTHI control) – (% killing of each sample) = relative % killing]. The graph plot replicates were derived from 4 healthy donors ± SEM. The statistical analysis was performed with One-way ANOVA and Dunett multiple comparison test. (** = $p < 0.01$, *** = $p < 0.001$).

Image of 11 day challenged chinchilla sections

Biofilms that had been allowed to form for eleven days within the middle ear of a chinchilla in an experimental model of otitis media induced by NTHI were recovered, as described in detail previously were used (Devaraj et al., 2021). Briefly, bullae which contained the NTHI biofilm adherent to the middle ear mucosa and associated PMNs that had migrated to the middle ear in response to the bacterial challenge were embedded in OCT (Fisher Scientific, Waltham, MA), cut into ten micron sections and labeled for IF imaging using rabbit anti-Z-DNA and/or mouse anti-B-DNA or their associated isotype control sera, then incubated with goat anti-rabbit conjugated to Alexa Fluor® 594 and/or goat anti-mouse conjugated to Alexa Fluor® 488. Sections were then coverslipped with Prolong Glass containing NucBlue as the mounting medium (Molecular Probes, Eugene, OR). Images were captured using a Zeiss LSM 800 with Airyscan.

QUANTIFICATION AND STATISTICAL ANALYSIS

Quantification of average thickness, fluorescence intensity, optical density, and absorbance values were determined as described in STAR Methods. Statistical significance was determined by either unpaired, paired t test, Tukey's multiple comparisons test, Dunnett's multiple comparison test, or One-way ANOVA with GraphPad Prism (version 8.0 and 9.1) and is described as appropriate, within the respective figure legends. A p value ≤ 0.05 is indicated by *, a p value ≤ 0.01 is indicated by**, a p value ≤ 0.001 is indicated by ***, and a p value < 0.0001 is indicated by ****. Error values represent the SEM.

CellPress
OPEN ACCESS

Supplemental figures

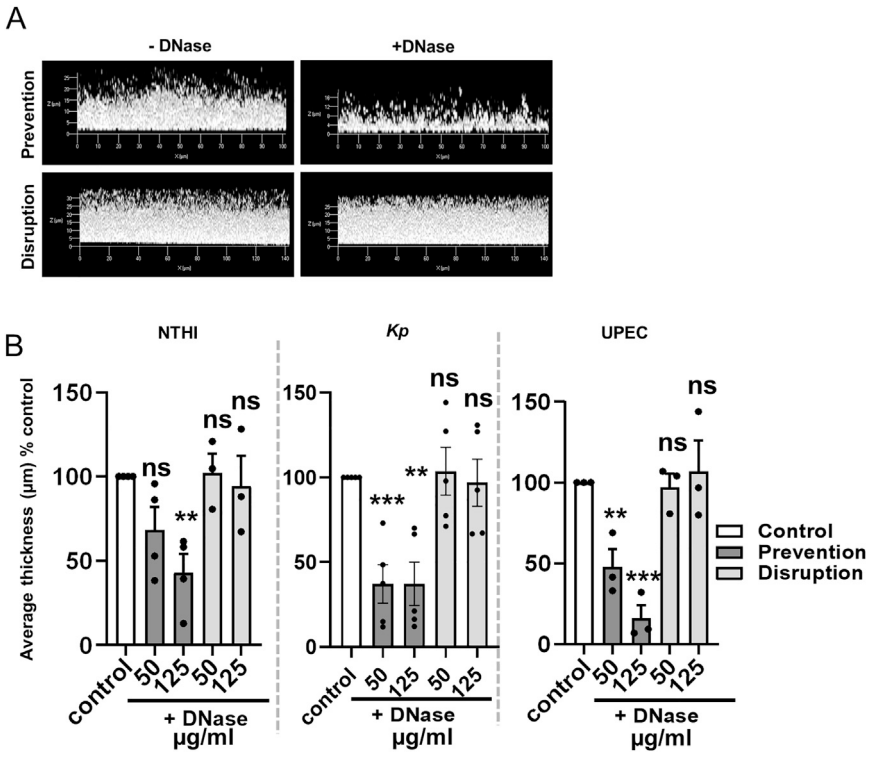

Figure S1. Mature biofilms were resistant to DNase, related to Figure 2

(A) Representative images of UPEC biofilms incubated with DNase. (B) Increasing concentrations of DNase were added at initial biofilm seeding of NTHI, Kp and UPEC (prevention of biofilm development) or 24h after seeding (disruption of mature biofilms). After DNase treatment, biofilms were incubated for an additional 16h, then stained with LIVE/DEAD® viability stain, fixed, visualized via CLSM, and images analyzed by COMSTAT. Error bars represent the standard error of the mean (SEM). Statistical significance of DNase treatment compared to control (- DNase) was assessed by unpaired t tests, $^{**}p < 0.01$ and $^{***}p < 0.001$. NTHI prevention, n = 4 and disruption, n = 3; Kp prevention and disruption, n = 5; UPEC prevention and disruption, n = 3. DNase inhibited the formation of biofilms by UPEC, Kp and NTHI, but did not disrupt these structures once formed.

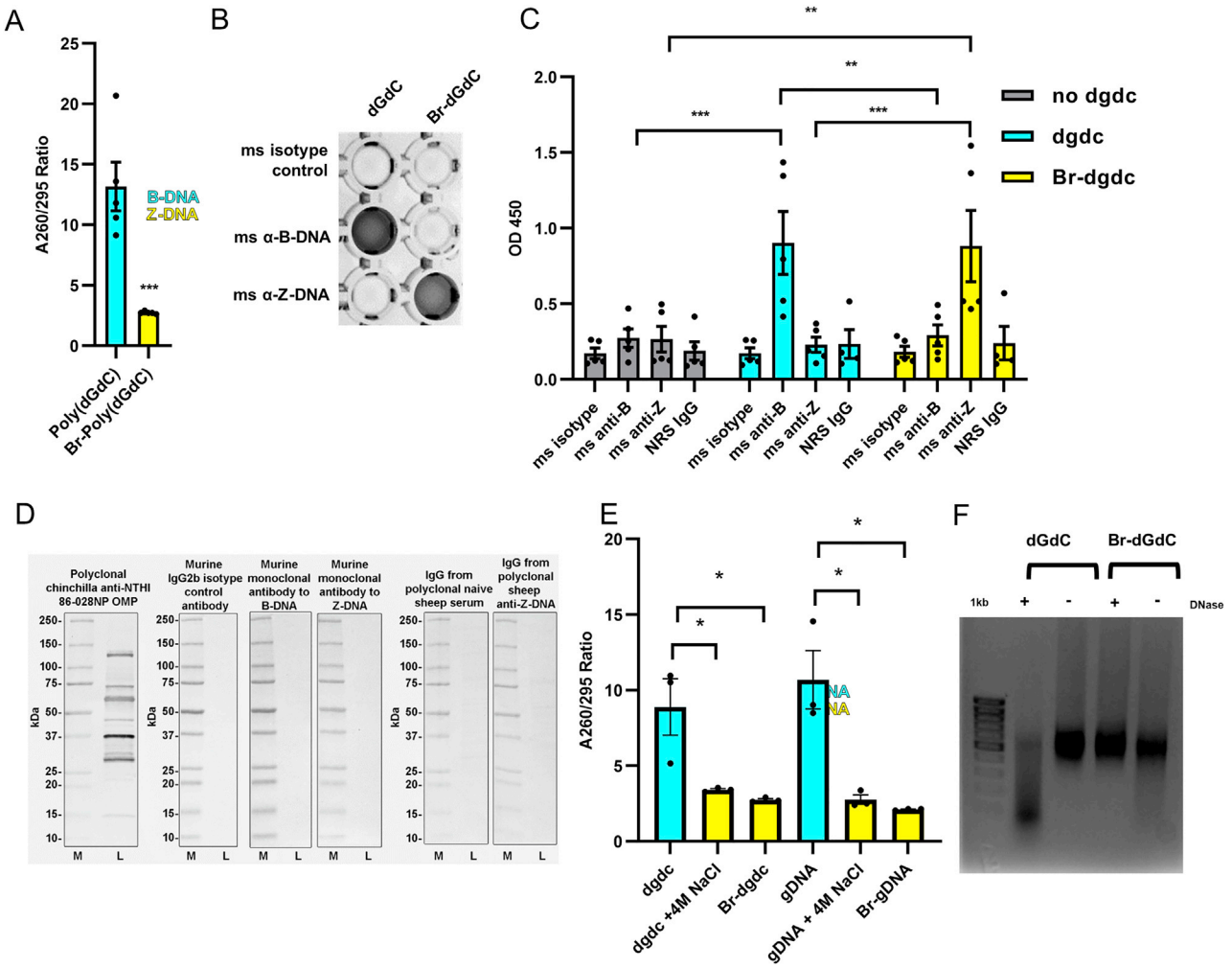

Figure S2. Verification of the specificity of B- and Z-DNA specific antibodies, related to Figures 1 and S5

(A) Brominated poly(dGdC) (10 μg/ml) or non-brominated poly(dGdC) (10 μg/ml) were incubated in buffer, the absorbance values at 260nm and 295nm were measured, then the A260/295 ratio was calculated. Poly(dGdC) had a ratio of 10.51 ± 1.33 indicative of B-DNA, while Br-poly(dGdC) had a ratio of 2.73 ± 0 which is indicative of Z-DNA. Statistical significance compared to control (non-brominated poly(dGdC) was assessed by unpaired t tests, ***$p < 0.001$, n = 3. (B) Representative ELISA plate image demonstrated the specificity of monoclonal antibodies to B- or Z-form DNA. An ELISA plate was coated with 1 μg of poly dGdC (B-DNA) or brominated poly dGdC (Z-DNA[102]), blocked with 0.5% (w/v) BSA, then probed with murine IgG1 (ms isotype) and naive rabbit serum (NRS) (neg. controls), or murine monoclonal antibody directed against B-DNA or Z-DNA (ms anti-B or -Z, respectively), followed by detection with a secondary goat α-mouse IgG-HRP. TMB (3,3′,5,5′-tetramethylbenzidine) was the colorimetric substrate used for HRP detection (dark gray wells). (C) Quantification of the ELISA for specificity of the B- and Z-DNA monoclonal antibodies. Statistical significance of murine α-Z-DNA and α-B-DNA were compared to control (no dGdC buffer) and assessed by Tukey's multiple comparisons test, **$p < 0.01$, ***$p < 0.001$, and $p < 0.0001$, n = 4. (D) Western Blot analysis of bacterial biofilm whole-cell lysates (L) (20 μg) probed with the indicated antibodies (M – molecular mass standards), n = 4. The monoclonal antibodies used in this study which are directed to B-DNA and Z-DNA are specific and do not cross react with bacterial lysates. (E) Brominated gDNA (4 μg/ml) or non-brominated gDNA (4 μg/ml) were incubated in buffer or 3.6M NaCl, absorbance values at 260nm and 295nm were measured, then the A260/295 ratio was calculated. Brominated Poly(dGdC) and non-brominated poly(dGdC) were used as internal controls. gDNA had a ratio of 10.69 ± 3.36 indicative of B-DNA. Conversely, Br-gDNA had a ratio of 2.19 ± 0.06 and gDNA 3.6M NaCl had a ratio of 2.76 ± 0.53 which are both indicative of Z-DNA. Statistical significance compared to control (non-brominated) was assessed by unpaired t tests, n = 3. (F) Poly(dGdC) and Br-poly(dGdC) were incubated in the presence or absence of Pulmozyme® (5U/ml) for 10 minutes at 37°C. The DNA degradation was assessed by gel electrophoresis which showed that Br-poly(dGdC) was protected from the activity of DNase, n = 3. ***$p < 0.001$. Error bars represent the SEM.

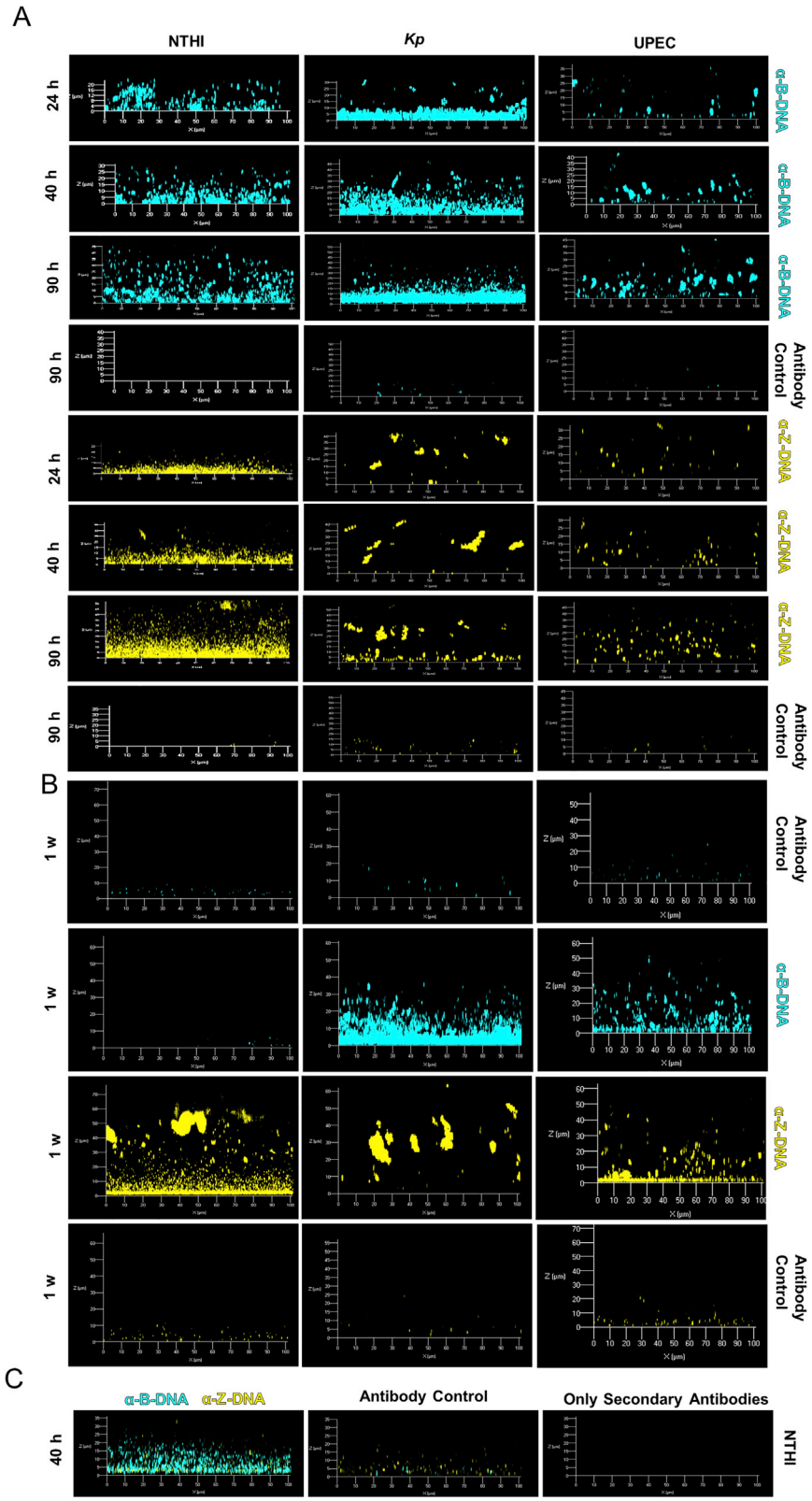

(legend on next page)

Figure S3. B-DNA and Z-DNA increased within the EPS of biofilms, related to Figure 1

(A) 24, 40, 90h, or (B) 1 week old NTHI, Kp, and UPEC biofilms were examined. Unfixed biofilms were incubated with a murine monoclonal antibody against either B-DNA (5 μg/ml) or Z-DNA (5 μg/ml), then revealed via incubation with goat α-mouse IgG conjugated to Alexa Fluor® 488. Biofilms were visualized by CLSM. B-DNA (cyan) and Z-DNA (yellow) accumulated as the biofilms matured, n = 3. (**C**) NTHI biofilms (40h) were incubated with the same primary, control antibodies, and buffer (no primary antibody), then visualized with the same secondary antibodies as described above, n = 3. No cross-reactivity of the secondary conjugated antibodies was observed.

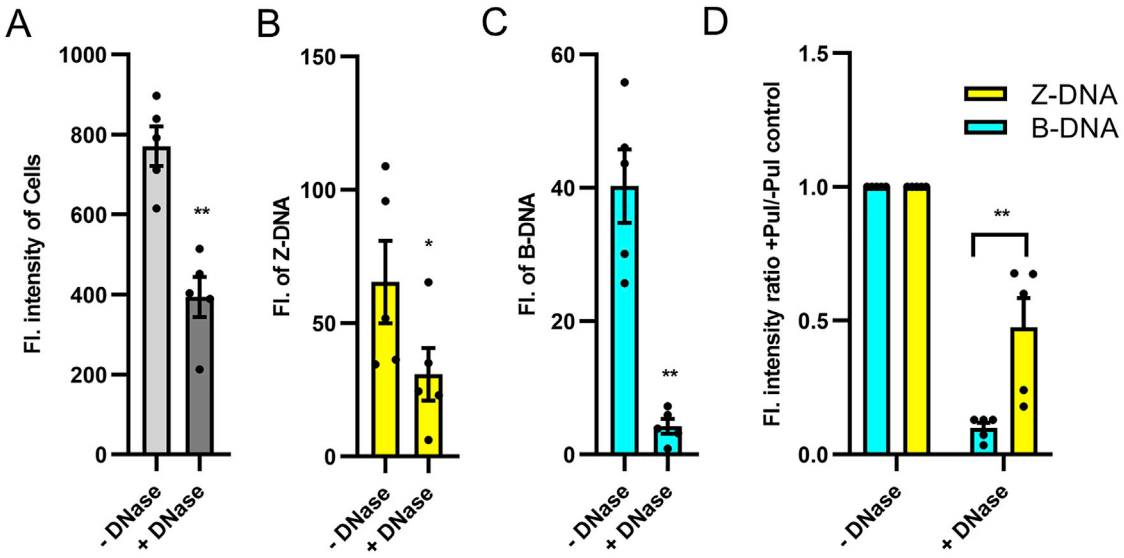

Figure S4. Removal of B-DNA throughout biofilm development reduced Z-DNA, related to Figure 2

NTHI biofilms were initiated in the presence or absence of DNase (80 U/ml) for 40h. Unfixed biofilms were incubated with a murine monoclonal antibody against either B-DNA[3519] (5 μg/ml) or Z-DNA (5 μg/ml), then revealed via incubation with goat α-mouse IgG conjugated to Alexa Fluor® 405 and goat α-rabbit IgG conjugated to Alexa Fluor® 488. Changes in either: (A) biomass (FM4-64 fluorescent signal); (B) Z-DNA (Alexa Fluor® 488) or (C) B-DNA (Alexa Fluor® 405) were quantified by ImageJ software. (D) The ratio of relative B-DNA to Z-DNA of IF intensity of DNase incubated biofilms were compared to the intensity of the media control. Error bars represent the SEM. Statistical significance compared to control (no DNase) was assessed by unpaired t tests, *$p > 0.05$ **$p < 0.01$, $n = 4$.

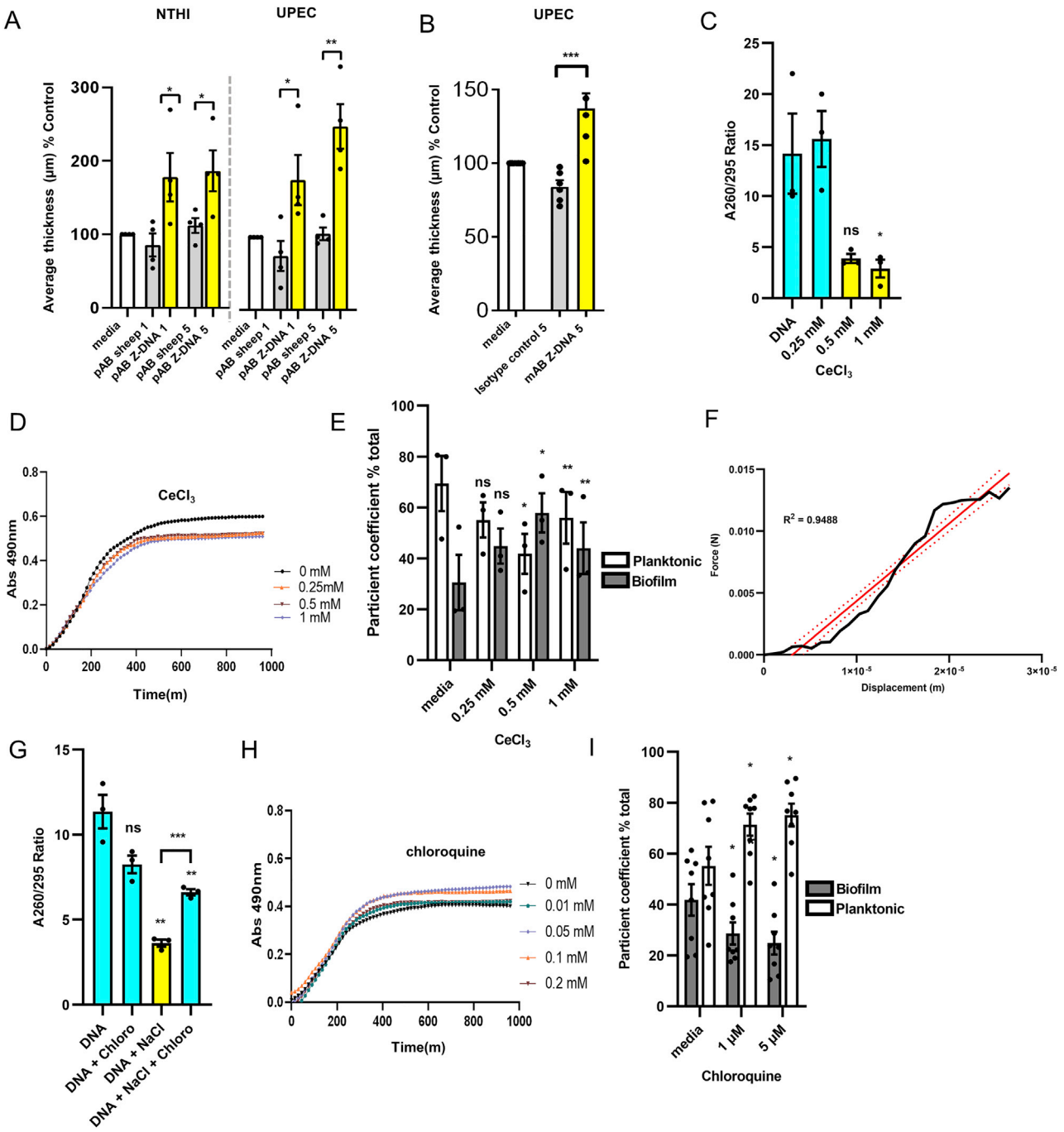

Figure S5. Z-DNA-specific antibodies stimulated biofilm formation, $CeCl_3$ induced Z-DNA, whereas chloroquine converted Z-DNA to B-DNA and partitioned planktonic NTHI differentially, related to Figures 3, 4, and S2

(A) NTHI and UPEC biofilms were initiated in the presence of increased amounts (1 or 5 μg/ml) of either IgG from unimmunized sheep serum (pAB sheep), sheep polyclonal α-Z-DNA (pAB-Z-DNA) or media for 16h, n = 4. (B) UPEC biofilms were initiated in the presence of rabbit monoclonal α-Z-DNA (mAB Z-DNA), rabbit monoclonal isotype 2b (isotype control) or media for 16h. Biofilm average thickness was analyzed by LIVE/DEAD® staining with COMSTAT image analysis. Error bars represent the SEM. Statistical significance compared to control was assessed by paired t tests, *$p < 0.05$, **$p < 0.01$, n = 6. (C) Genomic DNA isolated from NTHI (4 μg/ml) was incubated with increased concentrations of $CeCl_3$ (0, 0.25, 0.5, and 1 mM) in buffer, and analyzed by spectroscopic absorbance ratio assay. The ratio determined for samples that contained either 0 or 0.25mM $CeCl_3$ were 14.17 ± 6.79 or 15.61 ± 4.75 respectively, which indicated B-DNA. In contrast, ratios determined for 0.5 and 1mM $CeCl_3$ were 3.90 ± 0.76 or 2.90 ± 1.51, respectively, which indicated Z-DNA. Error bars represent the SEM. Statistical significance compared to control was assessed by unpaired t tests, *$p < 0.05$, n = 3. (D) Growth curves of NTHI grown planktonically in the presence of increased concentrations of $CeCl_3$ (0.25, 0.5, and 1 mM) indicated a minimal effect on growth (n = 3, averaged curves). (E) NTHI was allowed to form a biofilm for 24h in the

(legend continued on next page)

presence of $CeCl_3$. At 40h, relative CFU of the planktonic and biofilm populations were assessed to calculate the relative percent of planktonic versus biofilm resident NTHI which represents the 'partition coefficient', n = 3. (F) To determine the Young's modulus of treated and untreated NTHi biofilms, the slope of the lower linear portion of the force-displacement curve that corresponded to 0 – 40% strain (Figures 3 and 4), where $R^2 \geq 0.9$, was determined. Using the slope, the Young's modulus was calculated according to Equation S1. Depicted is the force-displacement region of a representative untreated control NTHi biofilm that corresponded to 0 – 40% strain. The linear fit of the curve is indicated in red; the dashed lines indicate the 95% confidence interval. The R^2 value of the linear fit is indicated. (G) Poly(dGdC) DNA (10 μg/ml) was incubated with 0.1 mM chloroquine, 3.6M NaCl or a combination of both, followed by analysis of the spectroscopic absorbance ratio assay. The absorbance 260/295nm ratios calculation for poly(dGdC) and 0.1mM chloroquine were 11.36 ± 1.72 and 8.25 ± 0.90 respectively which indicated B-DNA, while the ratio value calculated for 3.6M NaCl was 3.62 ± 0.37, which confirmed Z-DNA, n = 3. Chloroquine prevented NaCl- induced Z-DNA formation as determined by the ratio calculation of 6.61 ± 0.32. (H) Planktonic NTHI growth curves with increased concentrations of chloroquine (0.01, 0.05, 0.1, and 0.2 mM) indicated no effect on growth (n = 3, averaged curves). (I) NTHI was allowed to form a biofilm for 24h followed by the addition of increasing concentrations of chloroquine. At 40h, the partition coefficients were calculated, as above. Error bars represent the SEM. Statistical significance compared to control was assessed by paired t tests, *$p < 0.05$, n = 7.

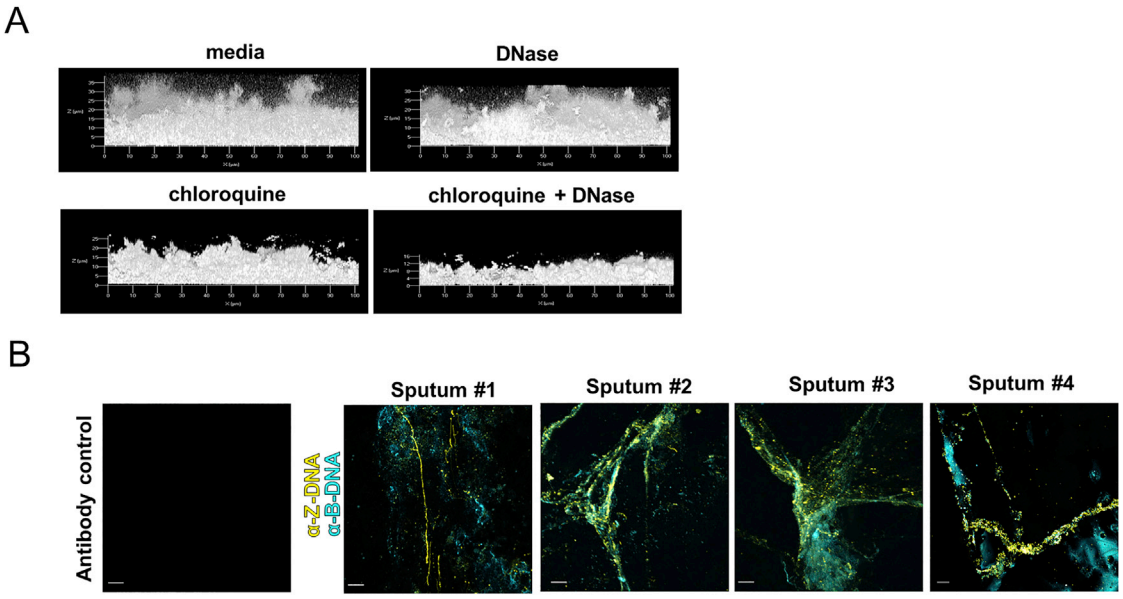

Figure S6. Modulation of B/Z eDNA increased the susceptibility of biofilms to DNase, related to Figure 3 and Table S1

NTHI biofilms were formed for 40h and incubated with chloroquine, DNase, or both, then stained with LIVE/DEAD®, fixed, visualized via CLSM, and images analyzed by COMSTAT, quantified in Figure 3K, n = 7. (A) Representative images of NTHI biofilms incubated with DNase and/or chloroquine. (B) Representative images of IF labeling of B-DNA with murine α-B-DNA[3519] and Z-DNA with rabbit αZ-DNA[Z22] in 4 unique specimens collected during exacerbation of clinical disease and assayed in Figure 3M, n = 1. Labeling was revealed with goat anti-rabbit IgG conjugated to Alexa Fluor® 647, goat anti-mouse IgG conjugated to Alexa Fluor® 488. Scale bar 10μm.

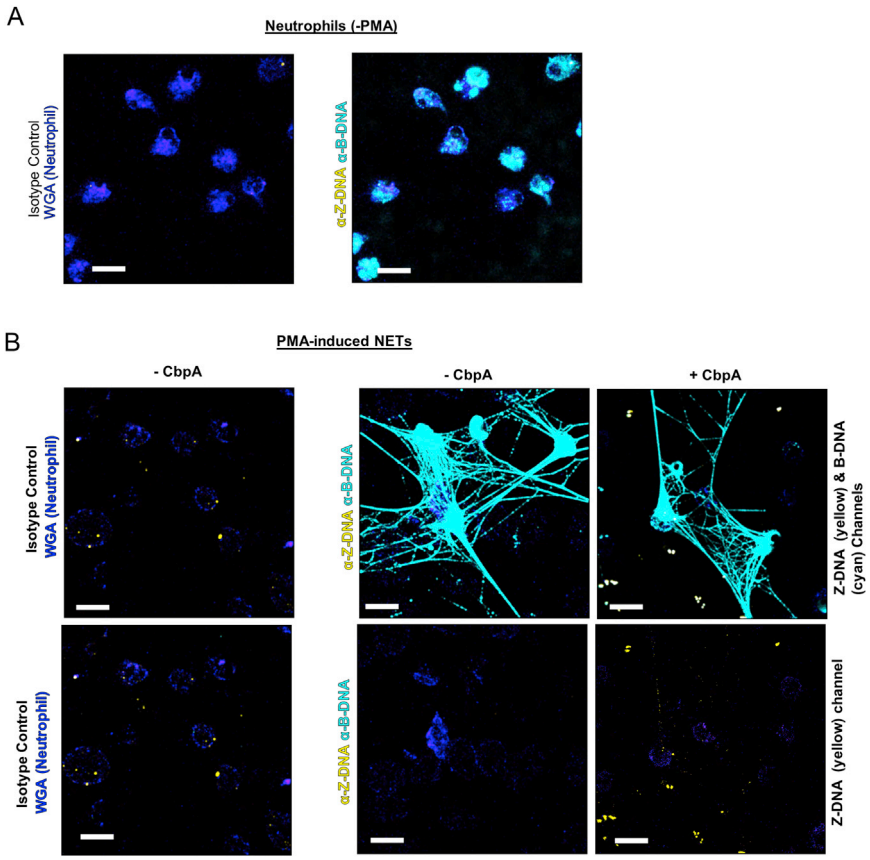

Figure S7. PMA-induced NET eDNA was predominantly comprised of B-DNA, related to Figure 5

Neutrophils ($1x10^5$) were allowed to attach to an 8 well glass chamberslide and incubated in the presence or absence of CbpA (500nM) upon induction with PMA (200nM) for 3.5h at 37°C. NETs were then fixed, washed, blocked with 10% goat serum followed by incubation with rabbit polyclonal antibody against human neutrophil elastase (1:100), rabbit monoclonal antibody against Z-DNA (5 μg/ml), and a murine monoclonal antibody against B-DNA (5 μg/ml). Then NETs were incubated with goat α-rabbit IgG conjugated Alexa Fluor® 594 and goat α-mouse IgG conjugated Alexa Fluor® 488, wheat germ agglutinin (WGA 350), and SYTOX nucleic acid stain. NETs were imaged by CLSM. (A) Representative image of no PMA control, n = 3. (B) Representative images of NETs formed in the presence or absence of CbpA (no Z-DNA induction), n = 3.